A cortico-subcortical loop for motor control via the pontine reticular formation

Emília Bősz[1, 2]†, Viktor M. Plattner[1, 3]†, Marco A. Diana[4] and László Acsády*[1]

Affiliations:

[1] Laboratory of Thalamus Research, Institute of Experimental Medicine; Budapest, Hungary

[2] János Szentágothai Doctoral School of Neurosciences, Semmelweis University, Budapest, Hungary

[3] Sainsbury Wellcome Ctr., London, United Kingdom

[4] Université Paris Cité, CNRS, Saint-Pères Paris Institute for the Neurosciences, F-75006 Paris, France

*Corresponding author: acsady@koki.hu

Laboratory of Thalamus Research, Institute of Experimental Medicine; Budapest, Szigony u. 43. 1083. Hungary

† These authors contributed equally to this work

Abstract

Movement control is governed by several parallel cortico-subcortical loops involving the basal ganglia (BG) and the brainstem. The BG loop is characterized by strong, excitatory input from the cortex, powerful, inhibitory output to the thalamus, and unilateral motor deficit following unilateral perturbation. In this project, we asked to what extent the glycine transporter 2-positive (GlyT2+) cells of the pontine reticular formation (PRF) form a circuit similar to the cortico-BG-thalamus loop. We found that layer 5 neurons of the secondary motor and cingulate cortical areas (M2/Cg) exert strong glutamatergic control over the PRF/GlyT2+ neuronal activity primarily via synaptic contacts on dendrites. Photoactivation of PRF/GlyT2+ neurons evoked decreased firing of their thalamic targets, and triggered movement initiation and unilateral rotation. These results demonstrate that the cortico-PRF-thalamus loop forms a cortico-subcortical pathway that regulates motor activity and shares certain structural and functional properties which are conceptually similar to the cortico-BG loop.

Introduction

Voluntary movements are controlled via diverse cortical and subcortical loops[1,2]. Among these, the cortex-BG-thalamus loop is one of the most intensively studied and is thought to be responsible for the planning, execution, and learning of complex motor sequences[2–5]. The input station of BG, the striatum, is contacted by dense, topographically organized inputs from almost all cortical regions[6–8]. These cortical afferents innervate mainly the spines of striatal medium spiny neurons and exert strong glutamatergic effects on their targets[9,10]. The output of BG targets several thalamic nuclei via large, multisynaptic, GABAergic terminals in rodents, carnivores and primates as well[11–13]. These BG efferents evoke pronounced inhibitory action on their thalamic targes and alter the firing activity[14–16]. Layer 5 cortical neurons that target the BG-recipient thalamus also innervate the BG, linking the input and output station of the cortico-BG loops[17]. Unilateral optogenetic interference with BG activity induces characteristic, unilateral rotation[4,18,19]. Similarly, unilateral injections of 6-hydroxydopamine (6-OHDA) or NMDA into BG output nuclei, as a model of Parkinson's disease, also causes unilateral motor deficit which results in asymmetric motor behavior and lateralized forelimb akinesia[20–23]. These structural and functional features of the cortico-BG loops allow highly diverse, plastic control of motor behaviors and suggest the involvement of BG in neurological conditions.

Several upper brainstem structures have recently been identified as key centers in movement organization[1,24–28]. To what extent the logic and function of the BG loops are similar to the midbrain circuits have not been systematically investigated, despite the fact that many of these regions are themselves under BG control. One of the largest midbrain nuclei is the pontine reticular formation (PRF). Like the BG, PRF also receives cortical

inputs[29] The output of PRF neurons expressing glycine transporter 2-positive (GlyT2+)[30] targets the thalamus via large, multisynaptic inhibitory terminals that are similar to BG boutons[29]. The termination zone of PRF/GlyT2+ neurons overlaps with the output of BG axons in the intralaminar and parafascicular nuclei (IL/Pf) of the thalamus[29,31] allowing the interaction of the two systems at the thalamic level. Photoactivation of PRF/GlyT2+ fibers in the IL/Pf resulted in a strong motor phenotype resembling akinesia, characterized by a loss of ability to move[29].

Based on these data in this study we tested the hypothesis that PRF/GlyT2+ neurons can represent a movement control system similar to BG in that they receive strong cortical inputs and exert unilateral rotational movements via inhibiting their thalamic targets. To this end we examined **i**; the cortical inputs to PRF and the impact of the cortex on PRF/GlyT2+ neuronal activity **ii**; co-innervation of PRF and the thalamic target region of PRF by the layer 5 (L5) cortical neurons, **iii**; the influence of PRF/GlyT2+ cells on thalamic activity in vivo, and **iv**; the ability of PRF/GlyT2+ cells to evoke rotational movements. We found that the cortico-PRF-thalamus loop shares some key structural and functional similarities with the cortico-BG-thalamus loop. We show that PRF/GlyT2+ cells receive strong cortical excitatory inputs, via cortical neurons that, in addition to PRF, also arborize in IL/Pf. The PRF/GlyT2+ cells can evoke pronounced inhibitory action on their thalamic targets in vivo and induce unilateral rotational movements. These findings suggest that the PRF/GlyT2+ cells are part of an alternative cortico-subcortical loop involved in motor control, distinct from the well-known cortico-BG loop[32].

Results

M2/cingulate cortical neurons innervate PRF/GlyT2+ neurons

In order to visualize cortical inputs to PRF/GlyT2+ neurons, we used anterograde virus-mediated tracing in RBP4-Cre::GlyT2-eGFP double transgenic mice. Flex-AAV-ChR2-mCherry virus injection into the secondary motor/cingulate (M2/Cg) cortical area labeled subcortically projecting layer 5 pyramidal cells (Fig. 1a-c). GlyT2+ cells were detected by eGFP expression[30]. Anterogradely labeled M2/Cg fibers formed a profuse axon arbor within the entire rostral PRF (Fig. 1d-f). The distribution of cortical afferents displayed significant overlap with the PRF/GlyT2+ neurons (Fig. 1d-f) but was not homogeneous within the PRF. A density map of cortical afferents showed a dorsomedial to ventrolateral decrease in fiber density within the PRF/GlyT2+ zone (Fig. 1g). Averaged maximum intensity projection of the density maps in 3 animals confirmed this gradient (Fig. 1h1-3). In addition, a rostrocaudal gradient was also observed in M2/Cg fiber density (Fig. 1h1-3, Supplementary Fig. 1). Caudal injections into the M2/Cg cortex (n=3) resulted in weaker PRF innervation (Fig. 1i). This data show that M2/Cg fibers innervate PRF in a topographic manner and are in position to innervate PRF/GlyT2+ neurons.

Next, we visualized M2/Cg fibers and PRF/GlyT2+ neurons using both high-power confocal imaging and high-power light microscopy using DAB/Ni (black) and DAB (brown) chromogens. With both methods, cortical afferents were in close proximity to GlyT2+ elements (Fig. 1j). We found putative synaptic contacts on the dendrites and occasionally on the somata of GlyT2+ neurons (Fig. 1k, l). In one case the spine of a PRF/GlyT2+ neuron, filled using the juxtacellular labeling method[33], was found to be contacted by an M2/Cg cortical terminal (Fig. 1m).

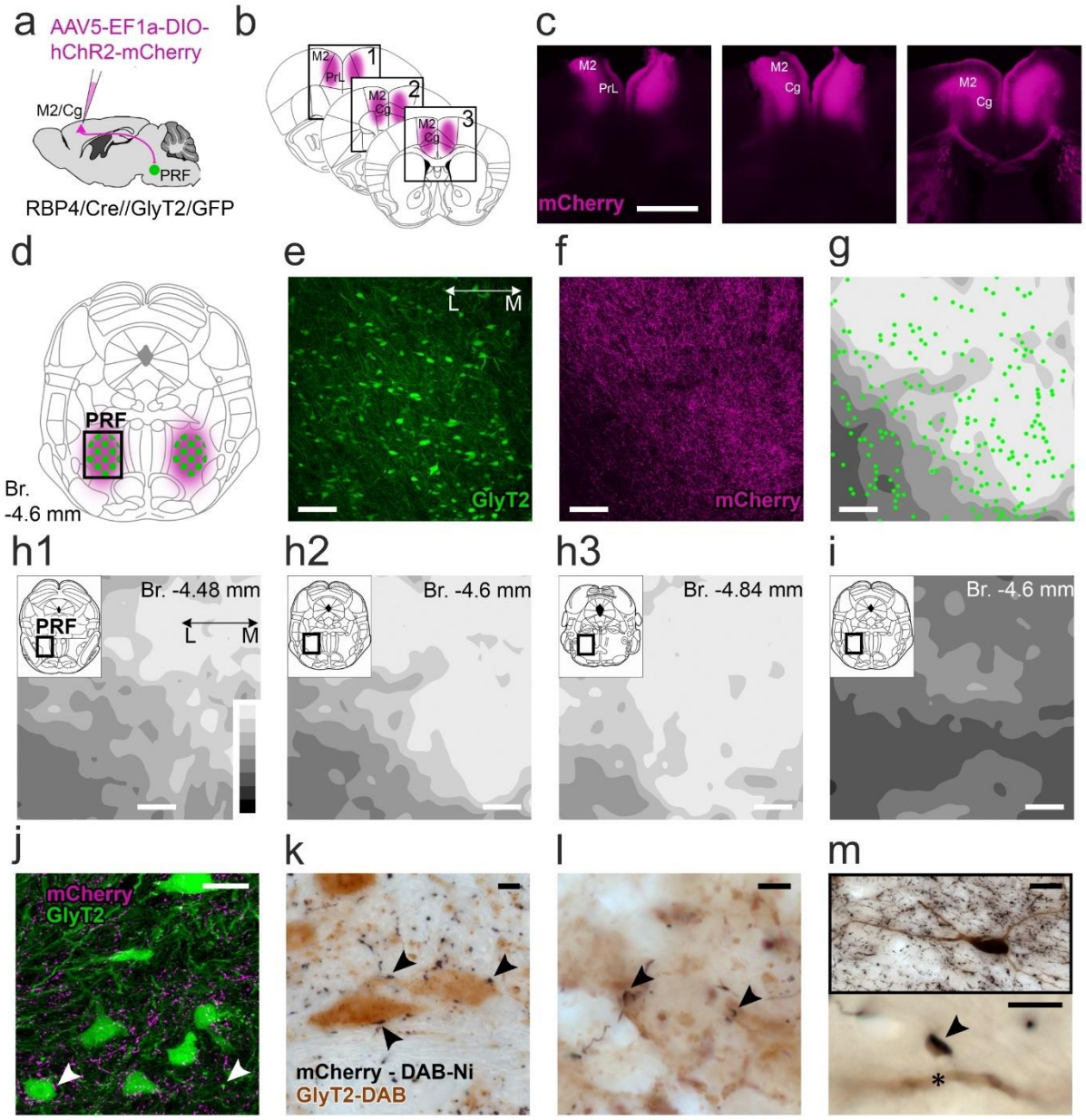

Fig. 1: Cortical inputs to PRF/GlyT2+ cells.

a) Scheme of anterograde tracing from the frontal cortical motor-related areas (M2/Cg) in the RBP4-Cre//GlyT2-eGFP mouse line (n=9 mice).

b) Schematic view of the injection sites.

c) Low-power fluorescent micrographs of the cortical injection sites at three anteroposterior levels.

d) Schematic view of the M2/Cg fibers (magenta shade) and PRF/GlyT2+ cells (green dots). The black rectangle, position of the micrographs and heatmaps in e-g.

e-f) Confocal micrographs (20x, n=5 mice) of the glycinergic cells (E) and anterogradely labeled M2/Cg cortical fibers (F) in the PRF glycinergic zone.

g) Fiber density heat map showing the distribution of cortical fibers (grey shading) and PRF/GlyT2+ cells (green dots). Higher fiber density is indicated with light grey colors.

h1-3) Maximum intensity Z projections of cortical fiber heat maps (n=3 animals) showing anterior M2/Cg inputs at three anteroposterior PRF levels extending from Br. -4.6 to Br. -4.84 (from the Paxinos atlas; 250µm)

i) Maximum intensity Z projections of cortical fiber heat maps (n=3 animals) showing posterior M2/Cg inputs.

j) High power confocal fluorescent image of anterogradely labeled M2/Cg fibers (magenta) and PRF/GlyT2+ neurons (60x, n=5 mice)

k-m) High power light microscopic image (n=9 mice) of close apposition between M2/Cg fibers (black) and the somata (k), dendrites (l), or a spine (m) of PRF/GlyT2+ neurons. Inset in m displays the juxtacellularly labeled PRF/GlyT2+ cell; arrowheads, cortical inputs; asterisk, spine.

Scale bars: c) 1 mm; e-i) 100 µm; j) 20 µm; k-l) 5 µm; m) 5µm, 20µm in the inset.

In order to identify the synaptic contacts formed by M2/Cg terminals in the PRF, we analyzed the ultrastructure of the M2/Cg synapses at the electron microscopic level (Fig. 2a-d). M2/Cg terminals were small to medium-sized (Supplementary Fig. 2), contained 1-

3 mitochondria, and established asymmetrical synapses with 1-2 active zones mainly with dendrites (Fig. 2b-c). The postsynaptic elements have variable diameters. Using double immunocytochemistry in 10 cases we identified synaptic contacts between virus-labeled cortical afferents and PRF/GlyT2+ neurons (Fig 2d1-4). In 9 cases the postsynaptic structure was mid-caliber dendrite in 1 case it was a PRF/GlyT2+ spine. These data show that L5 neurons of the M2/Cg cortex form conventional synaptic contacts mainly with the dendrites of GlyT2+ neurons in the PRF.

Synaptic properties of the cortical inputs in PRF/GlyT2+ neurons

Next, we investigated the physiology of synapses formed by the cortico-PRF terminals in GlyT2 cells. In vitro, PRF slice preparations were made from RBP4-Cre//GlyT2-eGFP animals that received identical Flex-AAV-ChR2-mCherry M2/Cg injections than in the case of the anterograde tracing. Optogenetic activation evoked synaptic currents with brief (2-3 ms) flashes of blue light. At a recording potential of -60 mV, these triggered rapidly rising and decaying inward synaptic currents with averaged amplitude amounting to 48.6 ± 20.2 pA; Fig. 2e, bottom panel). The amplitude of these responses was not modified by bath application of the GABAergic/glycinergic synaptic blockers SR95531 (2 μM) and strychnine (10 μM), thus demonstrating their excitatory nature. When recorded at a holding potential of +50 mV (see methods), the EPSCs showed clearly slower decaying kinetics than at -60 mV (visible for one experiment in the blue top traces in Fig. 2e), consistently with the appearance of an NMDA receptor-mediated component at the depolarized potential (Fig. 2e, top panel, black traces). Bath co-application of NBQX (10 μM) and DL-APV (50 μM), led to almost complete inhibition of the synaptic responses to 5.6 ± 1.4 % of the control at -60 mV, and to 10.1 ± 3.0 % at +50 mV (Fig. 2e top red

traces), thus demonstrating the glutamatergic nature of the cortico-PRF/GlyT2+ inputs. The amplitude of the NMDA component, as measured at +50 mV, amounted to 68.7 ± 15.3 % of the AMPA component at -60 mV (Fig. 2e). Moreover, the AMPA rectification index (measured as the ratio between the AMPA component amplitudes at -60 mV and at +50 mV) amounted to 1.9 ± 0.3 (n = 17; Fig. 2e bottom), not distant from the theoretical value of 1.75 for a linear I-V curve (see Otsu et al., 2018). This strongly suggests *that* the AMPA receptors present at these synapses are calcium-impermeable in PRF/GlyT2+ neurons.

In control pharmacological conditions, we examined the dynamic behavior of the cortico-pontine glutamatergic responses with trains of 10 optogenetic stimulations at different frequencies (1 Hz, 5 Hz, 10 Hz and 20 Hz). Along the stimulation trains the synaptic responses in the PRF/GlyT2+ cells did not show a significantly depressing behavior, the amplitude of the responses to the 10th stimulation being significantly smaller than the one to the first light pulse only at 5 Hz (see top traces in Fig.2f). With respect to the first optogenetic stimulation, the amplitudes of the responses to the 10th light pulse were indeed 89.1 ± 11.5 %, 87.3 ± 8.2 %, 102.7 ± 5.7 %, 90.5 ± 14.0 % at 1 Hz, 5 Hz, 10 Hz, and 20 Hz, respectively (see bottom graph in Fig. 2f).

We also tested stimulation trains at 40 Hz. Here, the amplitude depression was more pronounced (albeit still not significantly different from the control). The 10th EPCSs amounted to 61.2 ± 12.0 % of the first response. It is nonetheless important to underline that this decrease might easily be explained by the poor efficacy and reproducibility of repeated activations of ChR2 at high frequencies[29]. Overall, these data confirm that the cortical inputs to the PRF/GlyT2+ neurons identified morphologically in the previous

sections are fully functional, and that they operate in a purely glutamatergic mode with little short-term depression.

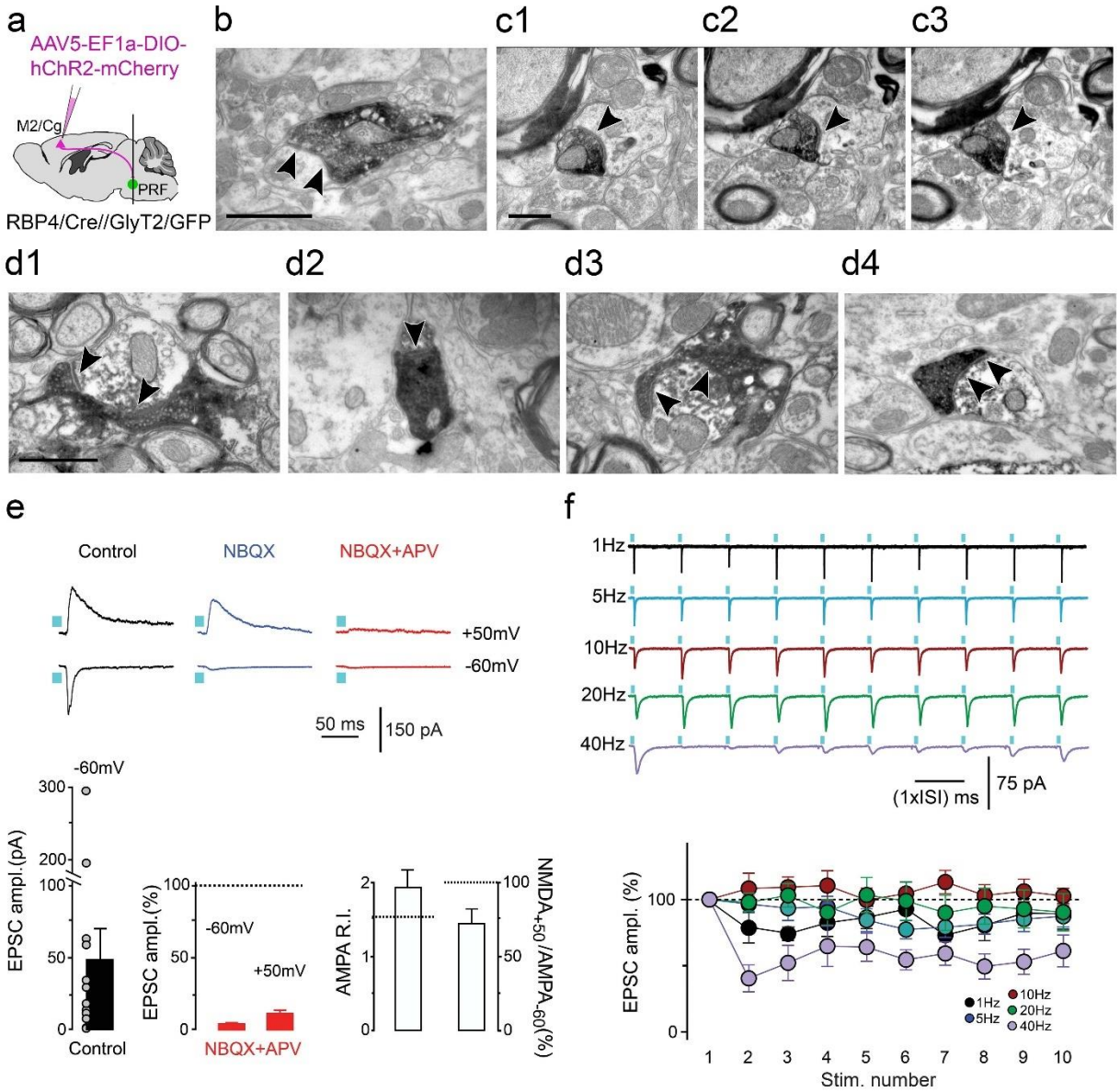

Figure 2. Cortical afferents target PRF/GlyT2+ cells and evoke a glutamatergic synaptic response.

a) Scheme of anterograde tracing from the M2/Cg in the RBP4-Cre//GlyT2-eGFP mouse line.

b-c) Electron micrographs of M2/Cg terminals (n=44, dark precipitates) in the PRF contacting mid-caliber dendrites (range: 0.197-1.437 µm, mean=0.62 µm, SD=0.31).

c1-c3) Serial EM images of the same axon terminal. Black arrowheads, synapses.

d) Electron micrographs of M2/Cg terminals (DAB-Ni, dark, dense precipitate) establishing synapses on PRF/GlyT2+ dendrites (n=9, D1, D3, D4, DAB, light precipitate) and spines (n=1, D2).

e) Optogenetically evoked (blue squares) AMPA and NMDA receptor-mediated components of the EPSCs elicited by M2/Cg terminals in the PRF. Traces from one exemplary experiment are shown above. Top: AMPA and NMDA components (n=16), control at -60 mV (n = 12; p = 0.002; Wilcoxon Signed-Rank Test) and at +50 mV (n = 12; p = 0.003; Wilcoxon Signed-Rank Test). Below, the graphs represent the results from all the experiments.

f) Top: Light-evoked EPSC-s displayed no significant depression during stimulation trains, at all tested frequencies ranging from 5 to 40 Hz. Bottom: 89.1 ± 11.5 % (n = 6; p > 0.05; Wilcoxon Signed-Rank Test), 87.3 ± 8.2 % (n = 14; p = 0.03); Wilcoxon Signed-Rank Test), 102.7 ± 5.7 % (n = 10; p = 0.7; Wilcoxon Signed-Rank Test), 90.5 ± 14.0 % (n = 12; p = 0.1; Wilcoxon Signed-Rank Test), 61.2 ± 12.0 % (n = 9; p > 0.05; Wilcoxon Signed-Rank Test) at 1 Hz, 5 Hz, 10 Hz, 20 Hz, and 40 Hz respectively.

Source data are provided as a Source Data file. Data are represented as mean +/- SE.

Scale bars: b) 1000 nm; c) 500 nm; d) 1000 nm.

The impact of cortical activation on PRF/GlyT2+ neuronal activity

In order to assess the impact of cortical inputs on the spiking activity of PRF/GlyT2+ neurons *in vivo,* we recorded the evoked responses of the PRF cells in ketamine-xylazine anesthetized animals (n=10 animals). In 7 cases we injected the flex-AAV-ChR2-mCherry virus into M2/Cg in the RBP4-Cre//GlyT2-eGFP double transgenic mice and photostimulated the L5 neurons (Fig. 3a-b). In 3 cases we applied bipolar electrical stimulation of the cortex in glyT2/GFP transgenic mice (5 ms pulse width, 1-2 mA) (Fig. 3a). In both stimulating conditions, we used trains of 1, 10, and 20 Hz stimulations (n=50 stimulus in 5 trains). To unequivocally identify and localize PRF/GlyT2+ neurons we used the juxtacellular recording and labeling methods [34]. Nine out of 10 neurons were recovered post hoc within the PRF and their GlyT2+ identity was determined by double fluorescent imaging (Fig. 3c, Supplementary Fig. 3a).

Cortical stimulation at 1 Hz generated reliable spike responses with short latency peaks, in all PRF/GlyT2+ cells (Fig. 3d, e) using both stimulation methods. Increasing the stimulation frequency to 10 and 20 Hz resulted in similar high-fidelity, fast responses (Fig. 3e, f). We found no significant difference between stimulation frequencies in response probability and latency (Fig. 3f) indicating reliable signal transmission even at high presynaptic activity. In order to assess the alteration of firing output of the PRF/GlyT2+ cells within the stimulation train at various input frequencies, we calculated the normalized evoked AP within a 50 ms time window after every stimulus (Supplementary Fig. 3b). The data demonstrated that the spiking activity of individual PRF/GlyT2+ cells did not depress within the stimulus train irrespective of the stimulation frequencies (Supplementary Fig. 3b). These in vivo data confirm the in vitro physiological data and show that frontal cortical

cells can evoke fast, reliable spike response on PRF/GlyT2+ cells even at high presynaptic stimulation frequencies.

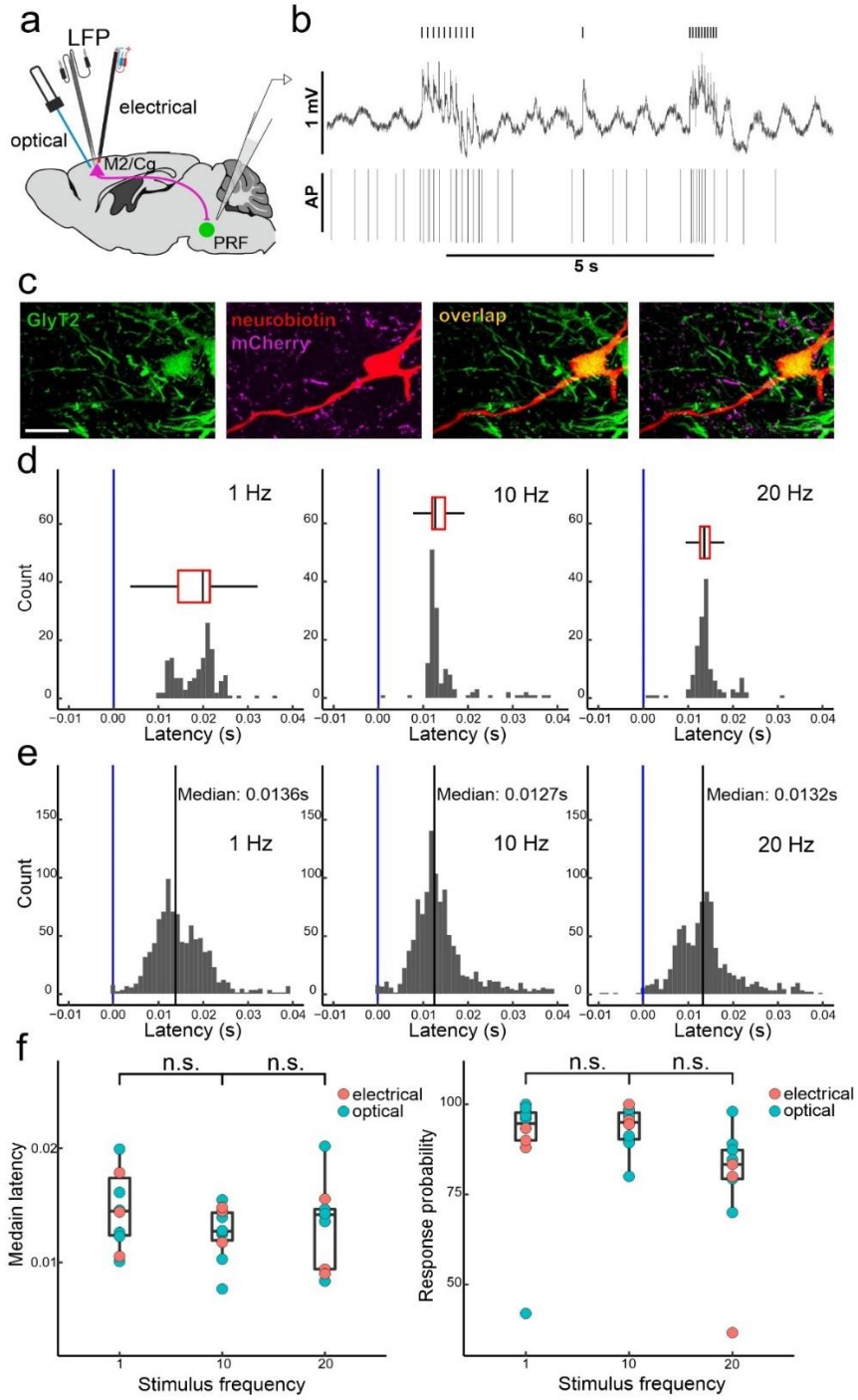

Figure 3. The effect of evoked cortical activity on PRF/GlyT2+ neurons

a) Scheme of the experiments (n=10 mice: 7 mice with optogenetic 5-ms-long pulses at 1-20 mW, 3 mice with electrical 5 ms pulses at 1-2 mA).

b) Representative stimulus-evoked cortical field activity and evoked firing of a glycinergic PRF neuron. Small ticks on the top indicate laser stimulation.

c) Representative fluorescent micrograph of a recorded and labeled PRF/GlyT2+ neuron. Green: GlyT2- eGFP; red: neurobiotin; magenta: M2/Cg fibers.

d) Peristimulus time histograms (PSTH) of cortical stimulus-evoked firing in a representative PRF/GlyT2 neuron at 1, 10, and 20 Hz stimulation frequencies. Response probability and median latency are visualized by box plots.1 Hz: probability 92.86%, 12.5 ms peak +/- SEM; 10 Hz: probability: 92.86%, 12.6 ms peak +/- SEM, 20 Hz: probability 84.06%, 14.5 ms peak +/-SEM.

e) Population PSTHs of juxtacellularly recorded and labeled PRF/GlyT2+ neurons (n=10) at 1, 10, and 20 Hz. 1 Hz median: 0.0136 s,10 Hz median: 0.0127 s, 20 Hz median: 0.0132 s.

f) Median latency (left) 1 vs. 10 Hz, n.s. p=0.22; 10 Hz vs. 20 Hz n.s. p=0.3, Mood's median test and response probability (right) 1 vs. 10 Hz, n.s p=0.59; 10 Hz vs. 20 Hz n.s. p=0.65 Mood's median test of the PRF/GlyT2+ neurons. Median latency 1 Hz mean: 0.015 s, SD: 0.003, median: 0.015; 10 Hz mean: 0.013 s, SD: 0.002, median: 0.013; 20 Hz mean: 0.013 s, SD: 0.004, median: 0.014. Response probability 1 Hz mean: 89.3, SD: 17.1, median: 94.7; 10 Hz mean: 93.4, SD: 5.96, median: 95; 20 Hz mean: 78.7, SD: 17.5, median: 83.3.

* $0.05<p<0.01$; ** $0.01<p<0.001$; *** $p<0.001$; n.s. - no significant difference. Source data are provided as a Source Data file. Scale bars: c) 20 μm.

Impact of spontaneous cortical activity on PRF/GlyT2+ cells

Earlier data indicated that the activity of PRF/GlyT2+ cells can be linked to different phases of slow cortical oscillations[29]. Here we asked to what extent the firing activity of PRF/GlyT2+ cells are sensitive to the alterations of cortical states (synchronized vs, desynchronized, Fig. 4., Supplementary Fig. 4., 5.). We recorded PRF/GlyT2+ neurons (n= 12) in GlyT2-EGFP transgenic animals and monitored the state changes in LFP activity (Fig. 4a, b). In case of 7 cells, we recorded spontaneous state changes between synchronized and desynchronized cortical states which can be observed in light ketamine-xylazine anesthesia (Fig 4b) whereas in 5 cases we evoked cortical inactivity by applying 2M potassium chloride (KCl) to the cortical surface to induce cortical spreading depression (Supplementary Fig. 6.) [35].

In the first experiments, we observed that 5 out of 7 PRF/GlyT2+ cells fired rhythmic AP clusters during the slow oscillatory periods (Fig 4b-d, Supplementary Fig. 5.). When the slow oscillation was replaced by a desynchronized period in the LFP, the firing pattern of the PRF/GlyT2+ cells immediately followed this transition and became irregular (Fig. 4b, d). When the rhythmic cortical activity was restored, the AP clusters reappeared (Fig 4b, d, Supplementary Fig. 5.). The transition from rhythmic AP cluster to tonic activity could be confirmed by autocorrelograms. (Fig. 4c.; Supplementary Fig. 4c). The mean rate of PRF/GlyT2+ action potential clusters was significantly higher in synchronized vs. desynchronized states (Fig 4d). The firing rate of PRF/GlyT2+ neurons significantly increased during the desynchronized states (Supplementary Fig. 4b). In the CSD experiments, cells decreased the rate of spike clusters upon cortical cell inactivation (Supplementary Fig. 6). These data demonstrate a tight connection between the cortical

states and firing activity of PRF/GlyT2 neurons and confirm the strong impact of cortex on these cells.

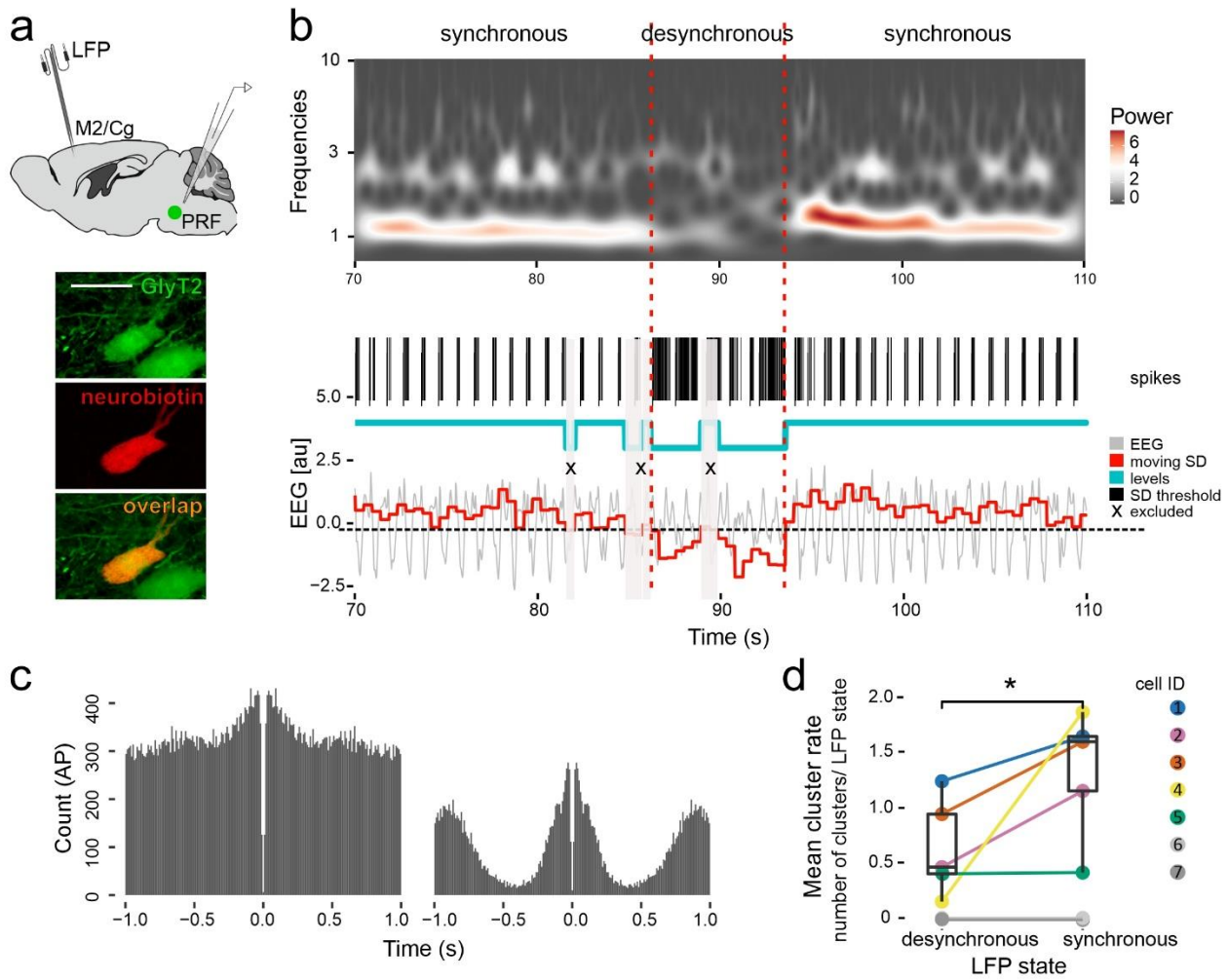

Figure 4. The effect of spontaneous cortical activity on PRF/GlyT2+ neurons

a) Scheme of the experiments (n= 7 mice) and a posthoc identified PRF/GlyT2+ (n=7, green) neuron filled with neurobiotin (red) and the overlapping (yellow) (bottom)

b) A representative example of a spontaneous state change under light ketamine-xylazine anesthesia together with the firing activity of a PRF/GlyT2+ cell.

Top: Wavelet transformation of the cortical LFP activity. Middle: Action potentials of a PRF/GlyT2+ cell, thick black lines correspond to the first action potential of the detected clusters. Blue line: synchronized and desynchronized states. Bottom: The raw LFP signal is shown in grey, the amplitude variance of the LFP signal (moving SD in a sliding window) is in red. The black dashed line represents the variance threshold for synchronized and desynchronized periods. Periods labeled with X (gray shading) are transient states, excluded from the analysis (see Methods).

c) Autocorrelogram of a representative neuron during synchronized and desynchronized periods.

d) Mean cluster rate (number of clusters/LFP state length) during synchronized (n=348, mean: 1.32, SD: 0.57, median: 1.59) and desynchronized periods (n=270). The two neurons shown in gray did not fire rhythmic AP clusters. (n=7, Wilcoxon Signed-Rank Test, p=0.032)

* 0.05<p<0.01; ** 0.01<p < 0.001; *** p<0.001; n.s. - no significant difference.

Source data are provided as a Source Data file. Scale bars: a) 20 μm.

Co-innervation of PRF and the thalamic targets of PRF by individual L5 neurons

L5 neurons that innervate the striatum have been shown to arborize in the thalamus[17]. Thus, next we investigated whether individual L5 neurons that target PRF can also innervate the target region of PRF/GlyT2+ cells in the thalamus (i.e., IL/Pf), potentially linking the activity of the source and the target regions.

In the Mouse Light Neuron Browser[36](https://www.janelia.org/open-science/mouselight-neuronbrowser) database we found 23 M2/Cg L5 neurons that had at least one axonal end point in the PRF (Fig. 5a-e; Supplementary Table 1.). Seventy-four percent of these neurons (n=17) projected to the IL/Pf as well. Ten out of the M2/Cg L5 17 neurons (59%) neurons co-innervating PRF and IL/Pf displayed multiple axonal end points (here defined as more than 4 end points) both in PRF and in the IL/PF. Four out of the 23 PRF projecting L5 neurons (17.4%) displayed very dense axonal arbors in PRF (more than 10 axonal end points) (Fig. 5f). Three of these L5 cells innervated IL/Pf also with more than 10 axonal end points. The fourth of them formed 6 end point in IL/Pf. Confirming our anterograde tracing experiments, these neurons arborized more in the dorsomedial part of the PRF (Fig. 5e-f). These data demonstrate that co-innervation of PRF and IL/Pf by the same cortical input neuron is frequent. L5 neurons that densely arborize in PRF tend to preferentially innervate IL/Pf with a rich axonal arbor.

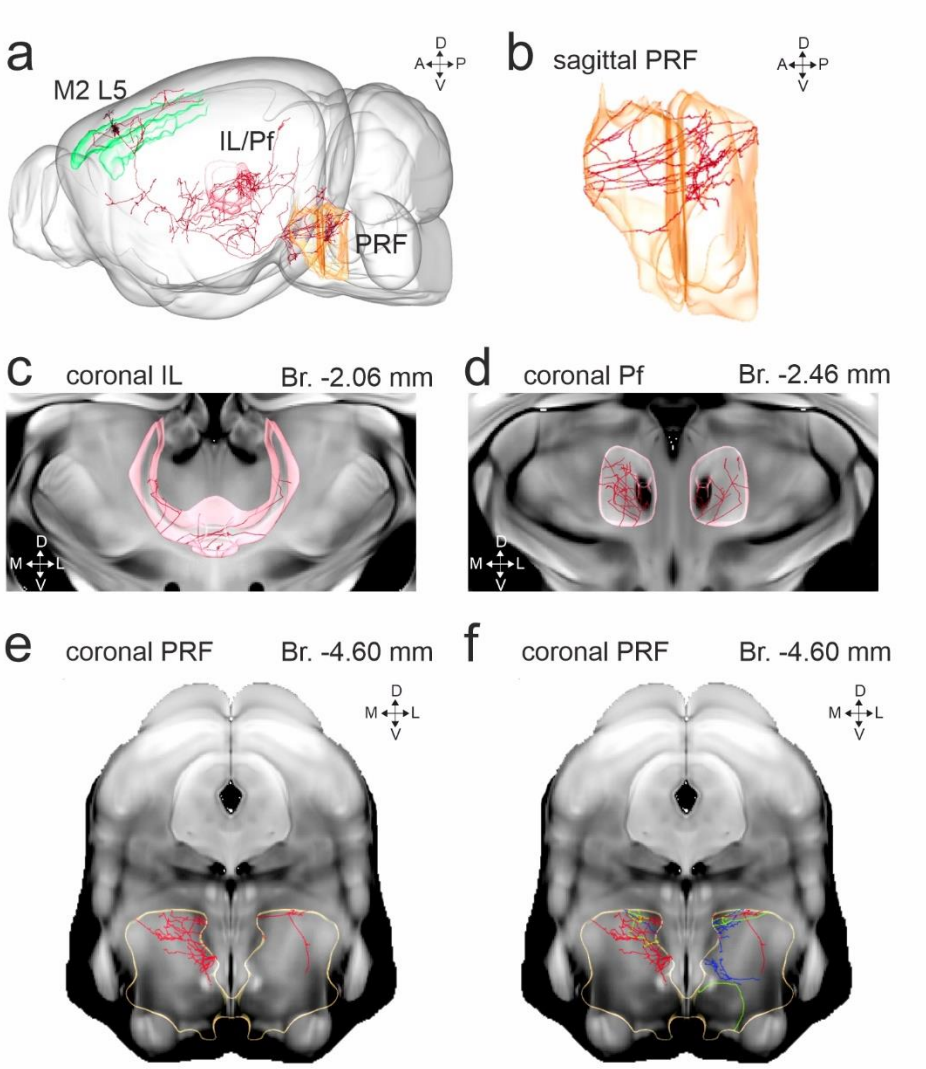

Figure 5. Co-innervation of PRF and thalamus by motor cortical L5 neurons

a) Reconstruction of a representative M2 L5 (AA0245) neuron from the Mouse Light Neuron Browser database which innervates both PRF and IL/Pf.

b) Axon arbor of the representative M2 L5 neuron (AA0245) at the sagittal level in the PRF.

c-e) Axon arbor of the representative M2 L5 neuron (AA0245) at one coronal level in the IL (c), Pf (d), and PRF (e, top). (e, bottom) Z-stack of all L5 axons in PRF.

f) Axon arbors of 3 L5 neurons in the PRF that have 10 or more axonal end points in the PRF and also innervate IL/Pf with multiple endpoints. Top, one coronal level; bottom, Z-stack of all axons in the PRF.

Activation of PRF/GlyT2+ neurons inhibit thalamocortical neuronal activity in vivo

PRF/GlyT2+ neurons have been shown to selectively innervate IL/Pf and evoke non-depressing, mixed, GABA/glycine receptor mediated IPSCs on their targets[29]. However, the effect of this inhibitory input on the spike output of IL/Pf has not been investigated. We performed in vivo juxtacellular recording and labeling experiments in GlyT2-Cre mice injected with flex-AAV ChR2-eYFP virus in the PRF (Fig. 6). PRF/GlyT2+ fibers were photoactivated in the IL/Pf (Fig. 6b). IL/Pf neurons are known to be sensitive to pain[37] thus we utilized urethane anesthesia to assess the impact of PRF/GlyT2+ photoactivation on spontaneous as well as tail-pinch-induced IL/Pf activity. Since it was important to determine whether the recorded IL/Pf neurons are located among the PRF/GlyT2+ fibers, the position of the IL/Pf cells was determined post hoc (Fig. 6a, d). The stimulation frequency used (33 Hz) was not higher than the spontaneous activity of PRF/GlyT2+ neurons measured under identical conditions[29].

The baseline mean firing rate (MFR) of the recorded thalamic neurons (n=23) varied between 1 and 30 Hz (Supplementary Fig. 7a). Tail pinch evoked a significantly higher MFR in the IL/Pf cells (Supplementary Fig. 7a). Optogenetic activation of PRF/GlyT2+ fibers (33 Hz) in the IL/Pf resulted in a significant decrease of IL/Pf spiking activity in both conditions at the population level (Fig. 6c, Supplementary Fig. 7c). The firing rate

immediately returned to baseline values at the cessation of stimulus trains (Fig 6c, Supplementary Fig. 7c).

Nineteen out of the 23 IL/Pf neurons (82.6%) were considered strongly inhibited (see Methods). In these neurons, inhibition of the firing output increased gradually and following a transient period of 1-2 seconds PRF/GlyT2+ inputs could almost entirely block the firing output of IL/Pf cells (Fig. 6e, Supplementary Fig. 7c). In 9 neurons we increased the duration of stimulation from 5 to 16 or 30 sec but the tonic cessation of firing was maintained even in these cases (n=9 cell) (Supplementary Fig. 7c). Firing activity returned to baseline levels after these long stimulations as well (Supplementary Fig. 7c). In the case of 4 out of the 23 IL/Pf neurons (16.7%), the PRF/GlyT2+ activation resulted in a brief gap (5-10 ms) in the PSTH immediately after the onset of the stimulus (Fig. 6f). The time course of this precisely timed inhibition corresponded well with the kinetics of the fast GABAergic/glycinergic IPSCs recorded during the earlier in vitro observations[29] indicating a fast, phasic inhibition in this subset of neurons. We recorded control neurons in the thalamus outside the PRF/GlyT2+ projecting zone. Activation of PRF/GlyT2+ fibers did not affect their firing activity (Supplementary Fig. 7c, d).

Nuclear localization of IL/Pf neurons inhibited by PRF/GlyT2+ activation was performed post hoc. IL/Pf cells were localized among PRF/GlyT2+ fibers in all cases (Fig. 6a). The recorded cells were distributed both in the anterior (centrolateral and paracentral) and the posterior (parafascicular) IL nuclei (Fig. 6d). All weakly inhibited cells were localized in anterior IL (Fig. 6d). We conclude that PRF/GlyT2+ neurons can exert a powerful effect on the spontaneous as well as tail pinch evoked firing activity of IL/Pf neurons and can

participate in both tonic (divisive) inhibitions as well as in timing the IL/Pf outputs by phasic inhibition.

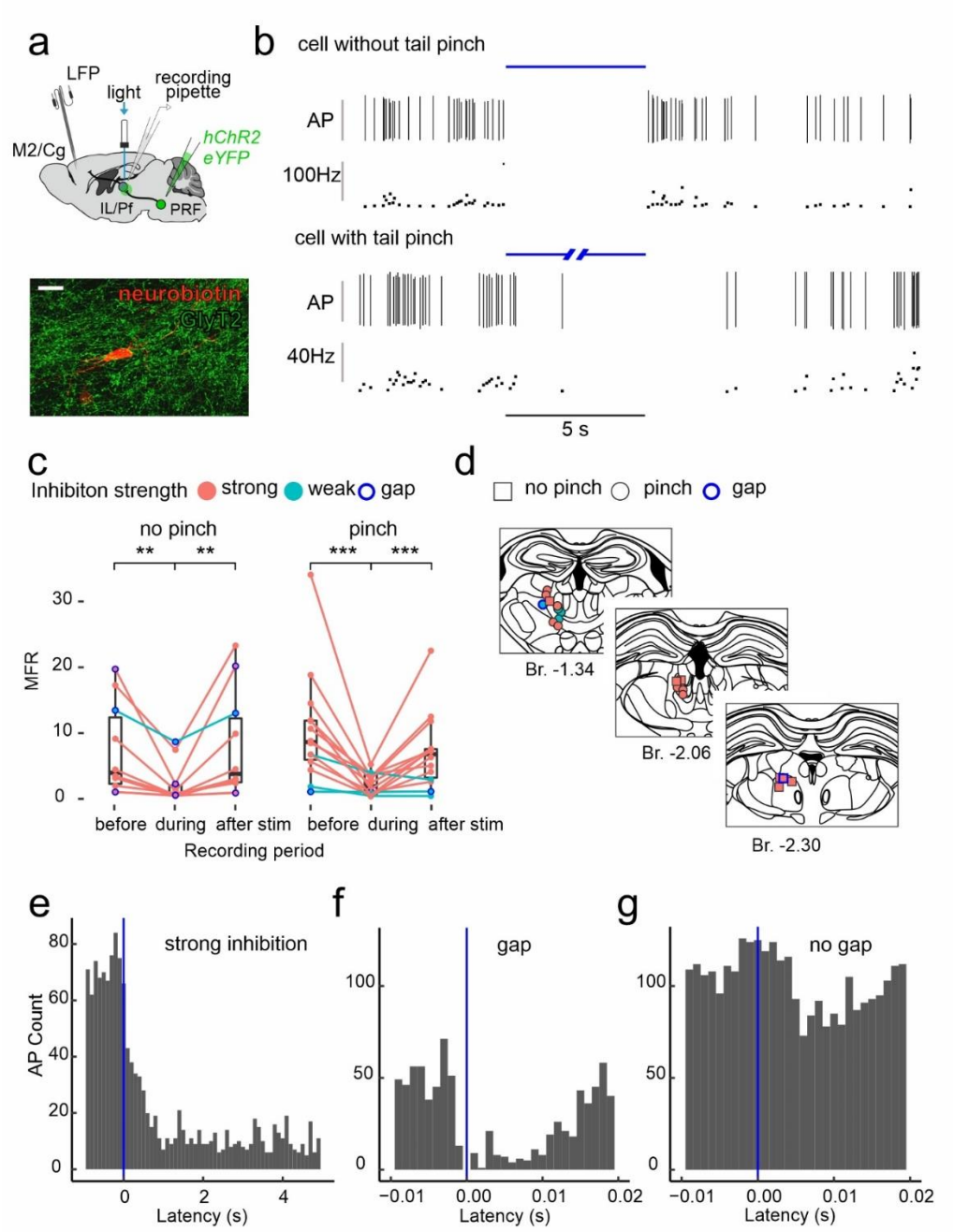

Figure 6. Inhibitory action of PRF/GlyT2 cells on thalamocortical cells in vivo

a) Top: Scheme of the experiments (n= 13 mice, n= 23 neurons). Bottom: Post hoc identified IL/Pf neurons surrounded by GlyT2+ fibers.

b) Response of two representative IL/Pf thalamic neurons to optogenetic activation of PRF/GlyT2+ fibers (top, 5 sec stimulation, without tail pinch, bottom, 30 sec stimulation with a tail pinch). Top: discriminated action potentials (AP), 5 sec stimulation, without tail pinch. Bottom: instantaneous firing rate (blue line = laser ON), 30 sec stimulation with a tail pinch.

c) Mean firing rate (MFR) of the recorded IL/Pf thalamic neurons before, during, and after the photoactivation PRF/GlyT2+ fibers. (33 Hz, 5 ms pulse width, laser power 10 mW, 5-30 sc duration). Strongly inhibited, weakly inhibited and gap cells are color-coded, strong (red, n=19 cell), weak (light blue, n=4, see Methods) inhibition, and neurons responding with a post-stimulus gap (dark blue circle, n=4) are indicated.

No pinch MFR before vs. stim p=0.002; no pinch MFR stim vs after p=0.002 n=10 cells; pinch before vs. stim p=0.00012; pinch MFR stim vs. after p= 0.00085, n=14 cells; Wilcoxon Signed-Rank Test.

No pinch before mean: 6.83, SD: 6.70, median: 3.47; no pinch during mean: 1.89, SD: 2.96, median: 0.381; no pinch after mean: 7.43, SD: 7.85, median: 3.30; pinch before mean: 9.62, SD: 7.98, median: 7.94; pinch during mean: 1.79, SD: 1.55, median: 1.52; pinch after mean: 6.44, SD: 5.44, median: 6.17.

d) Position of the recorded IL/Pf neurons in the thalamus. Same notation as in C. Rectangles are neurons recorded with tail pinch; circles are neurons without tail pinch.

e) Population PSTH of strongly inhibited IL/Pf neuron (n=19).

f) Short latency population PSTH of IL/Pf neuron with a post-stimulus gap in activity (n=4).

g) Short latency population PSTH of IL/Pf neuron without a gap (n=19).

* 0.05<p<0.01; ** 0.01<p < 0.001; *** p<0.001; n.s. - no significant difference. Source data are provided as a Source Data file. Scale bars: a) 20 μm.

Activation of PRF/GlyT2+ neurons promotes rotational movements

A characteristic response to unilateral excitation or inhibition of different cellular components of the BG is the occurrence of ipsi- or contralateral rotation[2,19,25,28,38]. A previous study has demonstrated that strong unilateral stimulation of PRF/GlyT2+ axon terminals in the IL/Pf induced immediate behavioral arrest[29]. However, there is currently no available data regarding the motor response to systematic, unilateral optogenetic activation of PRF/GlyT2+ cells. To measure the behavioral effect of activating PRF/GlyT2+ neurons we injected FLEX-AAV-ChR2-EYFP into the PRF in GlyT2-Cre animals and implanted fiber optics into the PRF. We photoactivated PRF/GlyT2+ neurons unilaterally (Fig. 7a) at various laser intensities (1; 5; 10; 15 mW; 5 ms pulse with, 40 Hz for 10 sec). Positions of the fiber optics were determined post hoc (Fig. 7b). For control, we injected the FLEX-AAV-EYFP virus into the same GlyT2-Cre animals.

First, we characterized movement initiation by the laser stimulation and its maintenance during the stimulation and measured traveled distance separately in the first second of the PRF/GlyT2+ stimulation and the subsequent 9 seconds. After the stimulus onset, we found significantly increased movement in the first second of the stimulus relative to the baseline period (before stimulus) with 3 stimulation intensities (1, 5 and 10 mW) but no significant change at the highest intensity 15 mW (Fig. 7c). Increased locomotion persisted in the remaining 9 sec of the stimulation (Fig. 7c). There was no significant dose-response effect with increasing laser light intensity (Supplementary Fig. 8a-b).

In the EYFP control animals, the mean traveled distance was not significantly different between the baseline and stimulation periods (Fig. 7d).

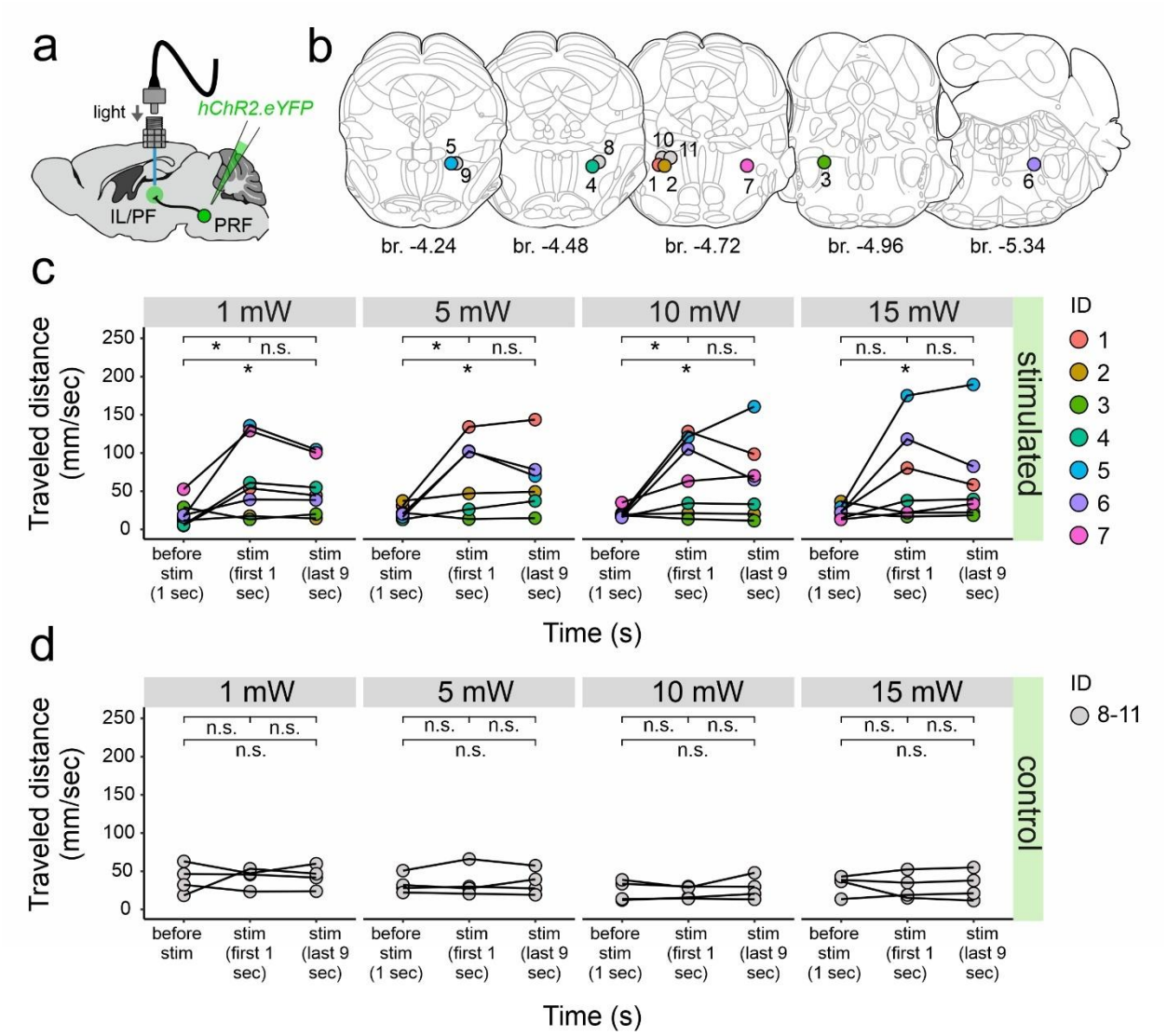

Figure 7. Photoactivation of the PRF/GlyT2+ neurons initiates locomotion

a) Experimental design of the photoactivation of PRF/GlyT2+ neurons (n=7 mice; at 1, 5, 10, and 15 mW; 5 ms pulse width, 40 Hz stimulation frequency, for 10 sec, n= 140 stimulation).

b) Schematic view of post hoc identified optic fiber position for experimental (colored dots) and control (grey dots) animals.

c) Comparison of the traveled distance (mm/sec) before the stimulus, in the first 1 sec and the subsequent 9 sec during the stimulus in the experimental animals. Before vs. first 1 sec p=0.023 at 1 mW, p= 0.031 at 5 mW, p=0.023 at 10 mW, p=0.055 at 15 mW; before vs. last 9 sec p=0.023 at 1 mW, p= 0.031 at 5 mW, p=0.023 at 10 mW, p=0.039 at 15 mW; first 1 sec vs. last 9 sec n.s. at 1, 5, 10, and 15 mW; Wilcoxon Signed-Rank Test. 1 mW before mean: 19.85, SD: 16.59, median: 16.20; 1 mW stim 1sec mean: 64.19, SD: 49.79, median: 53.85; 1 mW stim 9sec mean: 53.80, SD: 35.90, median: 44.41. 5 mW before mean: 23.21, SD: 9.16, median: 20.97; 5 mW stim 1sec mean: 70.84, SD: 48.54, median: 74.37; 5 mW stim 9sec mean: 65.47, SD: 44.55, median: 59.56. 10 mW before mean: 20.58, SD: 6.65, median: 18.49; 10 mW stim 1sec mean: 69.49, SD: 48.44, median: 63.17; 10 mW stim 9sec mean: 65.51, SD: 52, median: 65.03. 15 mW before mean: 22.96, SD: 8.12, median: 22.47; 15 mW stim 1sec mean: 67.34, SD: 60.50, median: 37.68; 15 mW stim 9sec mean: 63.42, SD: 59.85, median: 39.34.

d) Comparison of the traveled distance (mm/sec) before the stimulus, in the first 1 sec and the subsequent 9 sec during the stimulus in control animals. Before vs first sec: n.s. at 1, 5, 10, and 15 mW; before vs last 9 sec: n.s. at 1, 5, 10, and 15 mW; first 1 sec vs. last 9 sec n.s. at 1, 5, 10, and 15 mW, Wilcoxon Signed-Rank Test.1 mW before mean: 39.99, SD: 19.08, median: 39.30; 1 mW stim 1sec mean: 42.40, SD: 13.06, median: 46.46; 1 mW stim 9sec mean: 43.04, SD: 14.91, median: 44.22. 5 mW before mean: 33.28, SD: 12.39, median: 29.99; 5 mW stim 1sec mean: 35.99, SD: 20.40, median: 28.73; 5 mW stim 9sec mean: 35.87, SD: 16.55, median: 33.46. 10 mW before mean:

24.59, SD: 13.52, median: 23.69; 10 mW stim 1sec mean: 22.13, SD: 8.35, median: 22.18; 10 mW stim 9sec mean: 27.85, SD: 15, median: 25.12. 15 mW before mean: 32.95, SD: 13.22, median: 37.70; 15 mW stim 1sec mean: 30.39, SD: 17.004263, median: 26.97; 15 mW stim 9sec mean: 31.40, SD: 19.0, median: 29.52.

* $0.05<p<0.01$; ** $0.01<p < 0.001$; *** $p<0.001$; n.s. - no significant difference. Source data are provided as a Source Data file.

Next, we analyzed rotational movements during the stimulation of PRF/GlyT2+ neurons (10 sec) in the same animals (Fig. 8a-b; Supplementary Video 1-2). Rotational movements, as measured by mean rotational angle, significantly increased compared to the baseline periods at all stimulation intensities (1,5,10 and 15 mW) (Fig. 8c). In all but the weakest (1 mW) stimulation intensities rotational movements significantly decreased after the cessation of the stimulus (Fig. 8c). In the control animals, we found no significant changes in rotational angle during the stimulation (Supplementary Fig. 9a-c; Supplementary Video 3). There was no significant dose-response effect with increasing laser light intensity in either group (Supplementary Fig. 9d-e).

Interestingly, stimulation of PRF/GlyT2+ neurons induced contralateral rotational movements in 4 animals, and ipsilateral rotation was observed in the remaining 3 animals (Fig. 8d-e). Post hoc histological identification of optic fiber positions within the PRF revealed no discernible anteroposterior, dorsoventral, or mediolateral differences between the animals exhibiting ipsi- or contralateral rotational movements (Fig. 8e, Supplementary Fig. 9f-g).

In order to identify the effect of thalamofugal PRF/GlyT2+ neurons on rotational activity and compare it to the stimulation of the parent cell bodies, next we investigated the direction of rotational movements by stimulating PRF/GlyT2+ axons in its thalamic target (Pf). Similar to the activation of PRF/GlyT2+ cell bodies, stimulation of PRF/GlyT2+ fibers in the thalamus significantly increased rotational movements compared to the baseline periods (Fig. 8f; Supplementary Video 4). This rotational movement significantly decreased after stimulus termination (Fig. 8f). Stimulation of PRF/GlyT2+ axons in Pf always induced contralateral rotation (Fig. 8f-g). Bilateral stimulation in some of these cases (n=20 stim) or stimulation with higher (10-18 mW) laser intensity (n=24 stim) resulted in behavior arrest confirming data of a previous study[29]. These findings demonstrate that activation of PRF/GlyT2+ neurons is able to elicit rotational movements. The direction of rotation, however can differ depending on the stimulation site (somatic vs axonal stimulation).

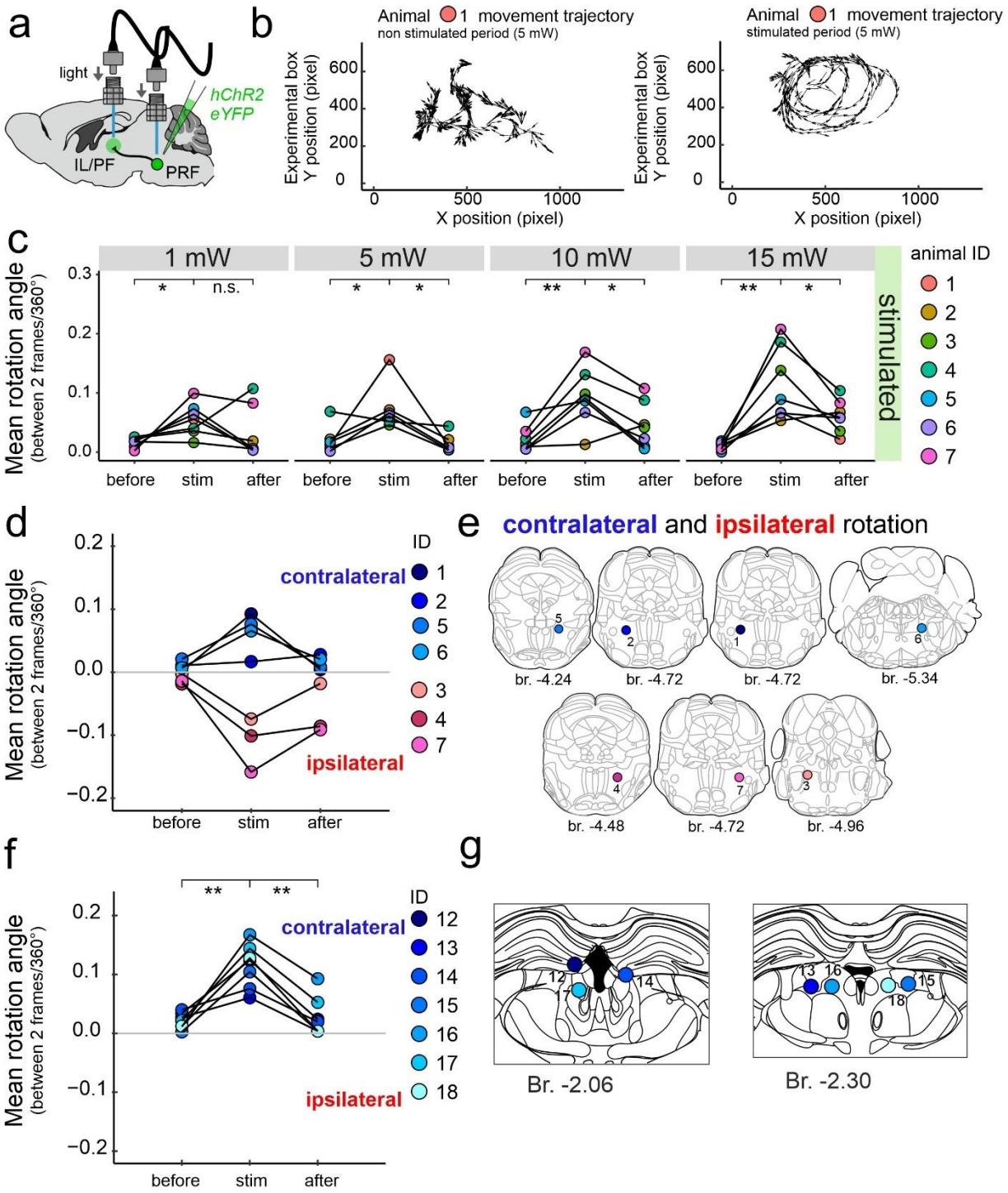

Figure 8. Rotational movements evoked by somatic vs axonal PRF/GlyT2+ photoactivation

a) Experimental design of the photoactivation of PRF/GlyT2+ neurons (n=7 fiber optic in n=7 mice) or their axons in Pf (n=7 fiber optic in 2 mice).

b) Movement trajectory in one representative mouse (mouse ID: 1) during the non-stimulated period (left) and the stimulated period (right) at 5 mW in the PRF.

c) Comparison of the absolute values of the mean rotation angle before, during and after the PRF stimulus periods in the 7 experimental mice. Before vs. stim p=0.016 at 1 mW, p= 0.031 at 5 mW, p=0.0078 at 10 mW, p=0.0078 at 15 mW; stim vs. after n.s. at 1 mW, p= 0.016 at 5 mW, p=0.016 at 10 mW, p=0.023 at 15 mW, Wilcoxon Signed-Rank Test. 1 mW before mean: 0.017, SD: 0.008, median: 0.018; 1 mW stim mean: 0.055, SD: 0.027, median: 0.056; 1 mW after mean: 0.033, SD: 0.043, median: 0.006. 5 mW before mean: 0.021, SD: 0.024, median: 0.015; 5 mW stim mean: 0.075, SD: 0.041, median: 0.063; 5 mW after mean: 0.014, SD: 0.015, median: 0.009. 10 mW before mean: 0.022, SD: 0.022, median: 0.014; 10 mW stim mean: 0.093, SD: 0.049, median: 0.091; 10 mW after mean: 0.046, SD: 0.039, median: 0.041. 15 mW before mean: 0.010, SD: 0.007, median: 0.012; 15 mW stim mean: 0.115, SD: 0.062, median: 0.089; 15 mW after mean: 0.061, SD: 0.028, median: 0.058.

d) Contralateral (n=4 animals) and ipsilateral (n=3 animals) rotations displayed as mean rotation angle before, during, and after the stimulus periods following PRF/GlyT2+ soma stimulation.

e) Schematic view of post hoc identified optic fiber position in PRF for the 7 experimental mice. Top: fiber optic positions induce contralateral rotation; bottom: fiber optic positions induce ipsilateral rotation. Same notation as in d).

f) Contralateral rotations (n=7 fiber optics) displayed as mean rotation angle before, during, and after the stimulus periods following PRF/GlyT2+ fiber stimulation in Pf. Before vs stim p=0.0078; stim vs after p=0.0078, Wilcoxon Signed-Rank Test. Before mean: 0.0213, SD: 0.013, median: 0.021; Stim mean: 0.115, SD: 0.038, median: 0.124; after mean: 0.029, SD: 0.033, median: 0.020.

g) Schematic view of post hoc identified 7 optic fiber positions for experimental animals in Pf.

* 0.05<p<0.01; ** 0.01<p < 0.001; *** p<0.001; n.s. - no significant difference. Source data are provided as a Source Data file.

Discussion

In this study we demonstrated that the PRF/GlyT2+ cells are under strong cortical control arising from higher order motor cortical regions. We also showed that PRF/GlyT2 cells can strongly reduce the spiking activity of their thalamic targets and induce unilateral rotational movements. Based on these data we propose that PRF neurons represent an important element of the upper brainstem locomotion complex. Below we compare the organization of cortico-PRF-thalamic loop to the cortico-BG-thalamic loop.

Cortical control of PRF/GlyT2+ cells

We found that M2/Cg L5 fibers innervate PRF in a topographic manner and establish synaptic inputs with mainly the dendrites of the PRF/GlyT2+ neurons. M2/Cg afferents evoked strong glutamatergic synaptic responses in PRF/GlyT2+ cells both in vitro and in vivo. A particular aspect of these experiments was that high frequency activations of the

afferents were followed by faithful synaptic or spiking responses with little depression under the in vitro and in vivo conditions, respectively. This suggests that the firing activity of PRF/GlyT2+ cells can be entrained by their cortical inputs. Indeed, spontaneous alteration in the level of cortical synchrony as well as the inactivation of cortical activity led to pronounced alteration of PRF/Glyt2+ firing activity.

Strong, topographically organized cortical afferents are the main features of the input station of BG as well[6–8,39]. Although earlier data reported markedly different spiking activity in cortex and striatum[40,41] in a particular situation recent data show that striatal activity can topographically reflect their cortical inputs[42]. The cortico-striatal synapses are subject to plastic changes which are thought to underly the acquisition of novel motor programs. This plastic alteration is attributed to innervation of striatal spines by cortical afferents[9,10]. In contrast to cortico-striatal connections spines were observed only occasionally as a target of cortico-PRF synapses indicating that this connection may be less plastic.

Cortex and BG form multiple nested loops since L5 cortical neurons that target the thalamus also innervate the BG. BG in turn using a strict topography, will finally contact the same thalamic region[6,8,39]. Using the Mouse Light Neuron Browser database we found a similar organization here. M2/Cg L5 neurons that arborized in PRF also innervated the thalamic target region of PRF/GlyT2+ fibers, IL/Pf. Although the role of integrating the direct cortical input with an indirect signal processed by a subcortical inhibitory center in the thalamus is presently unclear similar organization in two different motors systems highlights its importance.

Inhibitory action of PRF/GlyT2 cells on the thalamus

The activation of PRF/GlyT2+ fibers in the IL/Pf exerted significant inhibitory action on their thalamic targets *in vivo*. Two types of responses were distinguished, a gradual, tonic reduction in firing rate (divisive inhibition) upon repetitive stimulation and introduction of a brief gap, in the firing activity following each stimulus (phasic inhibition). The inhibited thalamic neurons were consistently found among the PRF/GlyT2+ fibers providing morphological evidence for a direct inhibitory action. The activity of thalamic cells outside the PRF/GlyT2+ axon arbor remained unaffected by the stimulation. Earlier in vitro data demonstrated non-depressing PRF/GlyT2+ IPSCs in PF/IL cells upon repetitive PRF/GlyT2+ stimulation[29]. This synaptic action can underlie the in vivo inhibitory influence observed in this study.

The existing evidence indicates that BG fiber activation can also evoke pronounced inhibition on their thalamic targets[14–16]. In functional essays it has been demonstrated that inhibitory action of BG on thalamus can alter the course of absence seizures[43] or to reduce the ramping activity in BG recipient thalamus during the delay period of a working memory task, resulting in impaired performance[44,45]

The strong inhibitory action of BG and PRF/GlyT2+ inputs on the thalamus are conveyed by axon terminals with strikingly similar features[13,29]. In both systems the individual axon terminals establish multiple synapses on a single proximal dendritic target. This synaptic arrangement allows interactions among the many release sites which probably underlies the strong inhibitory response recorded at these synapses in vitro, in vivo and under behavioral conditions[46,47]. The exact impact on network activity at these giant inhibitory

terminals is still not fully resolved[16,47]. In this study, in a subpopulation of Pf neurons a short gap in the firing activity was observed after PRF/GlyT2+ stimulations which is necessary for the “entrainment” model of BG action[16] on thalamus. Arborization of BG axon terminals and PRF/GlyT2 neurons[13,29,48] overlap in the IL/Pf nuclei allowing interaction between these two systems at the thalamic level and resulting in similar behavioral response upon stimulation (see below).

In conclusion the BG-thalamic and the PRF/GLyT2+-thalamic pathways share several similarities concerning their termination zone, the type of axon terminals and their effect on thalamocortical cells. Both systems may allow the selection and timing of an appropriate set of thalamocortical neuron required for a specific motor action.

Behavioral effects

Optogenetic activation of PRF/GlyT2+ cell bodies resulted in movement initiation and unilateral rotational movements. Activation of PRF/GlyT2+ fibers in the Pf also induced unilateral rotation. Rotational movement is a characteristic feature of the unilateral interventions that disrupt basal ganglia activity[4,18,22,23,49]. An imbalance or the co-activation of the direct and indirect pathways[4,19] or a unilateral lesion of dopaminergic fibers in the striatum all leads to rotation contralateral to the affected side[18]. This contrasts with the activation of the midbrain locomotor region (MLR) where unilateral stimulation of the glutamatergic MLR neurons results in symmetrical locomotion without a change in direction[27,28]. Therefore, it is unlikely that the observed effects are mediated via the MLR.

The specific neuronal circuit underlying contralateral rotation following BG interrogation is presently not clearly established. In case of an unilateral licking task[45,50]activation of

BG fibers in the thalamus induced contralateral deficits via impairing ipsilateral cortical activity. Similar mechanism may take place during the contralateral rotation observed in this study after the stimulation of PRF/GlyT2+ fibers in the Pf. Since the Pf region innervates both the motor cortical areas and the dorsal striatum[39,51,52] the activation of PRF/GlyT2+ inputs to Pf are able to disrupt the coordinated activity of ipsilateral thalamocortical and thalamostriatal motor circuits. Cortical motor output is known to cross the midline and target the contralateral spinal cord. Consequently, ipsilateral perturbation of motor thalamocortical neuronal activity will lead to contralateral perturbation of limb motility hence contralateral turning. Higher power unilateral PRF/GlyT2+ stimulation or bilateral stimulation in Pf led to the complete disruption of movements in agreement with previous data[29].

Contralateral turning could be elicited in only 4 out of the 7 animals following the stimulation of PRF/GlyT2+ cell bodies. In these cases similar mechanism may take place via the ipsilateral[29] ascending fibers of the PRF/GlyT2 cells to the thalamus. However, in three animals with PRF/GlyT2+ cell body stimulation, ipsilateral, not contralateral rotation was observed suggesting a different neuronal mechanism. The best characterized population of neurons associated with ipsilateral rotation is the CHX10-expressing, glutamatergic neurons projecting to the lumber region in the gigantocellular nucleus of the lower brainstem[53,54]. PRF neurons are known to project to the gigantocellular nucleus[55,56]. Thus, we hypothesize that, via a disinhibitory mechanism the activation of PRF/GlyT2+ cells could lead to increased firing of CHX10-expressing neurons and, consequently, ipsilateral rotation. This question clearly requires further investigation. Importantly, we did not find systematic differences in the localization of the optic fibers

inducing in ipsi- or contralateral rotation. This suggests that circuit elements responsible for ipsi- or contralateral rotation in the PRF are intermingled. These results align well with recent discoveries which demonstrate the modularity or granularity of basal ganglia and brainstem motor networks[2]. According to these data neuronal populations with specialized function in the brainstem can be located in close proximity and still can be involved in coordinating different types of motor program. Along this line it has been shown earlier that in the PRF stimulation sites which induce unilateral or bilateral atonia via the spinal cord are mixed[57] indicating that granularity[2] may apply to the PRF as well.

Conclusions

The BG display a highly complex intra- and internuclear information processing, which involves a multistep dimensionality reduction of the original cortical signal [2,58]. Such a complex circuit has not, as yet, been described within the PRF. Nevertheless, the present data show that aside from the internal organization, the two systems share several similarities in cortical inputs, thalamic outputs and unilateral motor control. The exact division of labor between BG and PRF/GlyT2+ cells as well as between PRF/GlyT2+ cells and the multiple excitatory brainstem systems described earlier[1,2,59] remain to be established but data, presented here, strongly argues that PRF/GlyT2 cells are important elements of the brainstem motor circuits.

Acknowledgement

We thank the Light Microscopy Center, the Electron Microscopy Center and the Virus Technology Unit at the Institute of Experimental Medicine for providing support for the experiments. Authors would like to thank Krisztina Faddi for their excellent technical assistance and to Csaba Dávid for his help in quantifying the cortical input density in PRF.

Funding

ERC Advanced Grant FRONTHAL, 742595 (LA)

European Union project within the framework of the Artificial Intelligence National Laboratory RRF-2.3.1-21-2022-00004 (LA)

Author contributions

Conceptualization: EM, PV, LA

Methodology: EM, PV, MD, LA

Investigation: EM, PV, MD,

Visualization: EM, PV

Funding acquisition: MD, LA

Project administration: LA

Supervision: LA

Writing – original draft: EM, MD, LA

Methods

Animal housing

All experimental procedures were approved by the Institutional Ethical Codex, Hungarian Act of Animal Care and Experimentation (1998, XXVIII, section 243/1998) and the Institutional Animal Care and Use Committee of the Institute of Experimental Medicine, Eötvös Loránd Research Network, Budapest and by the regulations of the European Union guidelines (directive 2010/63/EU). The experiments were performed in accordance with the National Animal Research Authorities of Hungary (PE/EA/877-7/2020). For the experiments, we used healthy, adult male mice (40-150 days). We used the following mice strains: GlyT2-Cre (Tg) - B6129F1 and Bl6Fx, Rbp4/cre//BAC_glyt2/GFP (TgTg) - C57Bl/6J, BAC_glyt2/GFP -C57Bl/6J[29]. Mice were entrained to a 12 h light/dark cycle with food and water available *ad libitum*. We performed animal research according to the 3R principles.

Surgeries

Anesthesia

For all experiments (anatomy, electrophysiology, optogenetics) the surgeries were done based on the following protocol. As anesthetics, mice received an intraperitoneal injection of ketamine (111 mg/kg, Produlab Pharma, #07/01/2302) and xylazine (4.3 mg/kg, Produlab Pharma, #07/03/2303). For the maintenance of the anesthesia, intramuscular injection of ketamine/xylazine was given every 30-50 min during the experiments. The head of the animal was fixed in a stereotaxic apparatus (David Kopf Instruments, Tujunga,

California 91042, Model 900 Small Animal Stereotaxic Instrument). In one experimental condition, during IL/Pf in vivo juxtacellular recordings, we used urethane anesthesia (0.12–0.15 g/100 g).

Virus injections and fiber optics implantations

For the anatomical investigations and in vitro and in vivo electrophysiological experiments, including labeling layer 5 pyramidal cells, we injected cre-dependent viruses into distinct brain areas. All stereotaxic tracer injections were performed using a glass pipette (intraMARK, 20-30-µm tip diameter, BLAUBRAND, injection flow: 25nl/min) connected to a syringe and a stereotaxic micromanipulator (Kopf Instruments). After injection, the capillary was left at the injection site for 5 min before slow withdrawal to allow diffusion and minimize backflow. The mice were perfused or were used for experiments following a 3–5-week survival time.

We used Rbp4/cre//BAC_glyt2/GFP (TgTg) mouse line (altogether n=23 mice) for the investigation of the cortico L5-PRF pathway (n=9 mice), *in vitro* electrophysiology *(*n= 7 mice), and *in vivo* electrophysiology (n=7 mice). For all these experiments a same virus injection design was used. We injected AAV5.EF1.dflox.hChR2(H134R)-mCherry.WPRE.hGH (based on Addgene plasmid #20297, UNC Vector Core) cre-dependent virus into the frontal cortex, M2/Cg (AP: Br.1 mm and 2 mm; ML: Br.0.5 mm; DV: 0.7 mm; bilaterally into 2-2 AP position, 4 injection/mouse). For *in vivo* electrophysiology L5 photoactivation, the optic fibers (100 µm, 0.22 NA) were positioned above the virus injection site (M2/Cg).

For the investigation of the PRF/GlyT2+-thalamic pathways altogether n=26 adult GlyT2-Cre male mice were used including the in vivo optogenetic behavioral (n=13) and electrophysiology (juxtacellular recording, n=13) experiments. For optogenetic activation of PRF/GlyT2+ cells we injected AAV5.EF1a.DIO.hChR2(H134R)-eYFP.WPRE.hGH (based on Addgene plasmid #20298, UNC Vector Core) or for control AAV5.EF1a.DIO.eYFP.WPRE.hGH (based on Addgene plasmid #27056, Penn Core) virus into the PRF of GlyT2-Cre mice unilaterally (AP:-4.4, ML:0.8, DV: 4.2, 100 nl). For optogenetic activation of PRF/GlyT2+ fibers in the IL/Pf we did the same injections in a bilateral way.

After virus injection the optic fibers (Thorlabs, FG105UCA, Ø105 µm core, 0.22 NA) were implanted into the PRF (n=7 optic fiber in n=7 mice, AP:-4.4, ML:0.8, DV: 4.2) or IL/PF (n=7 optic fiber in n=2 mice, AP:-1.9 or 2.3 mm; ML: -0.8 mm; DV: -2.5 or -2.8 mm). Mice recovered from surgery and the viruses could transfect the PRF/GlyT2+ cells for 3 weeks before behavioral testing or juxtacellular recording. The optic fibers were labeled with DiI stain (1,1'-Dioctadecyl-3,3,3',3'-Tetramethylindocarbocyanine Perchlorate ('DiI'; DiIC18(3); ThermoFisher Scientific, #D282).

Histology

Perfusion and tissue fixation

Perfusions were performed under deep anesthesia (sodium pentobarbital 60 mg/kg). Using saline and a fixative solution (0.1% glutaraldehyde (wt/vol) (Electron Microscopy Sciences, #16210) and 4% paraformaldehyde (wt/vol) (TAAB Laboratory, #P001) in 0.1

PB. A peristaltic pump perfused the solutions through the ascending aorta. After the fixation, the brain was sectioned using a vibratome (50 µm coronal slices).

Immunohistochemistry

For all immunostaining methods, we used TBS buffer. The sections were incubated in sucrose solutions for cryoprotection and were frozen above liquid nitrogen to help the penetration of the antibodies, followed by BSA treatment (4% 40 min). To visualize the L5 fibers (ChR2-mCherry viral tracer) we used a rabbit anti-mCherry primary antibody (1:4000, BioVision, Inc., 23 California 95035, #5993-100, overnight). To label GlyT2+ cells and fibers in the PRF and in the IL/Pf (in the case of eYFP containing viral tracers or in the Rbp4/cre//BAC_glyt2/GFP mouse line), the sections were treated with chicken anti-eGFP primary antibody (1:15000, ThermoFisher, #A10262).

For light and electron microscopic analysis when we visualized the L5 fibers in the brainstem after the anti-mCherry primary antibody we used anti-rabbit ImmPRESS (1:2, Vector Laboratories Burlingame, Ca 94010) and DAB-Ni/DAB (DAB-Ni: Nickel-intensified 3,3′-diaminobenzidine (bluish-black reaction product), DAB: 3,3′-diaminobenzidine, Sigma-Aldrich, #D5637, brown reaction product) as a chromogen. In the other case, after the anti-eGFP primary antibody (1:15000, ThermoFisher, #A10262) we used ABC (avidin biotinylated horseradish peroxidase complex, 1:300, Vector Laboratories, #PK-4000) and DAB as a chromogen.

For fluorescent and confocal microscopic investigations of L5 fibers, after the anti-mCherry primary antibody, we used Cy3-conjugated goat anti-rabbit secondary antibody (1:500 Jackson RRID: AB_2313593; Code: 111-167-003). In the case of the anti-eGFP

primary antibody, we used the anti-chicken-Alexa488 secondary antibody (1:500, ThermoFisher, #A-11039) to investigate GlyT2//eGFP components.

After juxtacellular recordings neurobiotin was visualized with Cy3-conjugated streptavidin (1:2000, Jackson RRID: AB_2337244; Code: 016-160-084) in the PRF or in the IL/Pf. The GlyT2+ neurons/fibers and the cortical axons were visualized using the same histology mentioned above so we developed DAB-Ni/DAB or fluorescent immunostaining respectively.

To localize the fiber optics and juxtacellularly labeled cells, check virus injections, and analyze the fibers in the PRF, all micrographs were taken with OLYMPUS BX61, FLUOVIEW FV1000 confocal microscopy (software: Olympus Fluoview 1.6) or with ZEISS AxioPlan2 fluorescent microscopy with OLYMPUS DP70 camera (software: Olympus DPController 1.2.1.108) or Zeiss Axio Imager M1 microscope coupled to an AxioCam HrC digital camera.

Electron microscopy

To analyze the M2/Cg terminals' ultrastructure, we performed immunostaining for the ChR2-mCherry viral tracer (DAB, as described above). To confirm the innervation of PRF/GlyT2+ neurons from M2/Cg, we performed double immunostaining for the ChR2-mCherry viral tracer (DAB-Ni) and GlyT2+//eGFP (DAB) and processed the material for EM. In our hands, the modified DAB-Ni precipitate in the axon terminals could be unambiguously differentiated from the end product of marble-like DAB.

After double immunohistochemistry of L5 terminals and PRF/GlyT2+ cells the sections were treated with OsO_4 (0.5%, vol/vol, with 7% sucrose for 40 min in 0.1 M PBS), followed

by dehydration, sequential incubation in ethanol, uranile acetate, and acetonitrile for ultrastructural analysis. The dehydrated sections were embedded in Durcupan (Sigma Aldricht, #44610Aldrich). Blocks containing PRF were re-embedded and sectioned to ultrathin sections (60 nm thick) with an Ultramicrotome (EM UC6, Leica Biosystems). The dendrites and terminals (area, diameter) were measured in three non-consecutive sections in FIJI software[60].

The sections were examined using a HITACHI 7100 electron microscope; the electron micrographs were taken with a Megaview digital camera.

In vitro electrophysiology

The *in vitro* electrophysiological experiments of Fig.2 were performed on coronal slices from the brains of PRF of adult mice (more than 3 months old), see the virus injection method in the previous paragraph.

Slices were prepared for a minimum of 4 weeks following surgery. Briefly, mice were anesthetized with an intraperitoneal injection of pentobarbital, then perfused through the ascending aorta with cold (2°-5°C) bicarbonate-buffered saline (BBS) containing (in mM): 115 NaCl, 2.5 KCl, 1.6 $CaCl_2$, 1.5 $MgCl_2$, 1.25 NaH_2PO_4, 26 $NaHCO_3$ and 30 glucose. Mice were then decapitated, and the portion of the brain containing the PRF was extracted and placed in BBS at 2°-5°C for a few minutes. Slices (300 µm) were then cut with a ceramic blade on a 7000smz-2 vibratome (Campden). The slicing procedure was performed in an ice-cold solution containing (in mM): 130 potassium gluconate, 15 KCl, 0.05 EGTA, 20 Hepes, 25 glucose, 1 $CaCl_2$ and 6 $MgCl_2$ supplemented with D-APV (50 µM). Slices were then transferred for a few minutes to a solution containing (in mM): 225

d-mannitol, 2.5 KCl, 1.25 NaH_2PO_4, 25 $NaHCO_3$, 25 glucose, 1 $CaCl_2$ and 6 $MgCl_2$, and finally stored for the rest of the experimental day at 32°-34° C in oxygenated BBS (pH 7.4 after equilibration with 95 % O_2 and 5 % CO_2). For all recordings, slices were continuously superfused at 32°–34° C with oxygenated BBS.

We recorded GFP-positive neurons from the pontine reticular formation (PRF; [29]). PRF identification was facilitated by the presence of the red fluorescent plexus originating from the cortical viral injections, observed via a 530 nm green LED (Thorlabs). Cells were visualized with a combination of infrared Dodt contrast and an on-line video contrast enhancement, using a CoolSnap HQ2 CCD camera (Photometrics) run by MetaMorph (Universal Imaging). Fluorescent glycinergic neurons were identified using a 470 nm-wavelength blue LED (Thorlabs). Both 470 nm and 530 nm LEDs were coupled to the slice chamber via the epifluorescence pathway of the microscope.

Whole-cell, voltage clamp recordings were performed with an EPC-10 double amplifier (Heka Elektronik) run by PatchMaster software (Heka). Patch pipettes (resistance 2-3 MΩ) were filled with an intracellular solution containing (mM): 110 $CsMeSO_3$ (Sigma), 4.6 $MgCl_2$, 10 HEPES, 10 K_2-creatine phosphate (Calbiochem), 10 TEA-Cl (Sigma), 0.05 4-AP (Sigma), 4 Na_2-ATP, 0.4 Na_2-GTP, 1 QX-314 (Tocris), pH 7.35 with CsOH (~300 mOsm). Series resistance was partially compensated (max 65%), whereas liquid junction potentials were not corrected. Stimulation train recordings were performed at a holding potential of -60 mV. The AMPA and NMDA components of the EPSCs were examined at both -60 mV, and +50 mV. The brief (2–3 ms long) flashes of blue light used to evoke synaptic responses were provided by triggering the 470 nm LED. TEA-Cl (500 μM) and 4-AP (50 μM) were added to the perfusing BBS when the AMPA and NMDA

components were investigated. This procedure was necessary both for increasing synaptic release probability, and for reducing the sizeable current leaks developing at +50 mV in control recording conditions, thus decisively improving EPSC detection.

In vivo electrophysiology

Cortical activation and LFP recording

For in vivo investigation of the L5-PRF pathway we activated the M2/Cg L5 cells optogenetically (see above the surgery details in Surgeriess n=7) and electrically (in BAC_Glyt2/GFP mice, n=3). The laser beam was generated by a 473 nm laser (Thorlabs lasers). The laser pulses were 5 ms long, 10 mW intensity, and were delivered at 1,10 and 20 Hz frequencies (n=50 stimulus in 5 trains). When we applied electrical stimulation (1-2 μA) we used a bipolar stimulating electrode on the surface of the cortex (M2/Cg, same position described above).

To record cortical field potentials, bipolar LFP electrodes (FHC, resistance ~1 MΩ) were inserted into the frontal cortex of mice (Bregma 1.7 mm; lateral -0.8 mm). The recorded signal was amplified, band-pass filtered from 0.16 Hz to 5 kHz for LFP recordings and from 100 Hz to 5 kHz to record the multiunit activity (Supertech BioAmp, Supertech, Pécs, Hungary) and digitized at 20 kHz (micro 1401 MkII, CED, Cambridge, UK).

Juxtacellular recording

PRF and IL/Pf single unit activity was recorded via glass microelectrodes (in vivo impedance of 20-40 MΩ) made from borosilicate glass capillaries (1.5 mm outer diameter, 0.75 or 0.86 inner diameters, Sutter Instrument Co., Novato, CA, USA or WPI Inc. Sarasota, Fl, USA). Electrodes were positioned into the PRF (Bregma -4.4 mm; lateral -

0.8 to -1 mm; ventral from cortical surface -3.8 to -4.8 mm) or IL/Pf (Bregma -1.9 to 2.3 mm; lateral -0.8 mm; ventral from cortical surface -2.5 to -2.8 mm) (using a piezoelectric microdrive (Burleigh 6000 ULN or ISS 8200, EXFO, Quebec City, Quebec, Canada). Neuronal signals were amplified by a DC amplifier (Axoclamp 2B, Axon Instruments/Molecular Devices, Sunnyvale, CA, USA), further amplified, and filtered between 0.16 Hz and 5 kHz by a signal conditioner (LinearAmp, Supertech) and recorded by Spike2 5.0 (CED). The electrodes were filled with 0.5 M K+- acetate and 2% neurobiotin (Vector Laboratories, Burlingame, CA, USA, #SP-1120). Juxtacellular labeling of the recorded neurons was done by filling the neurons with neurobiotin, as described in[33] . After the experiments, the animal was perfused, and coronal sections were cut from the whole brain (3.1. Perfusion and tissue fixation). To visualize neurons filled with neurobiotin and to determine their GlyT2 content (in the PRF) or whether it is surrounded by PRF/GlyT2+ fibers (in IL/Pf), we treated the sections as described in 3.2. Immunohistochemistry. The GlyT2::eGFP positivity was determined by confocal microscopy.

Cortical spreading depression

The local application of 1M potassium chloride (KCl) or tetrodotoxin (sodium channel inhibitor) induced CSD. The onset of cortical activity suppression happened after a few minutes and lasted for 15-20 minutes. To facilitate the normalization of cortical activity the cortical surface was rinsed with saline several times.

Janelia Mouse Light Neuron Browser

We analyzed single-cell reconstruction data of the Mouse Light Neuron Browser[36] (https://www.janelia.org/open-science/mouselight-neuronbrowser) by identifying PRF

projecting M2/Cg L5 neurons, we selected neurons that have their soma in M2 or Cg area and projected to the PRF. In the browser, we could set the threshold to the axonal projection, called the in the browser “axonal endpoint”. We used 4 thresholds: >=10, 5-10, 2-5, or 1. We always precisely checked the anatomical region to uniform terminology that we used during our research (Paxinos atlas vs Neuron Browser).

Behavior

Experimental protocol

After virus injection and optic fiber implantation (see above) the experimental protocol included handling (2 weeks), habituation (3 days), and the optogenetic experiment. The handling period started 1 week after the surgery. During the habituation, we placed the mouse in the experimental box and connected their optic fiber to a fiber optic patchcord (Thorlabs) and the patchcord cable (Thorlabs). The mice moved freely in the experimental box and got used to the new environment and the weight of the cable and the mouse was allowed to move passively. During the experiment phase, we photoactivated the transfected PRF/GlyT2+ cells or their fibers in IL/Pf. The photoactivation was generated by a 473 nm DPSS laser (LRS-0473-PFM-00050-03, Laserglow Technologies, Toronto, Canada). The photostimulation trains were 10 s long, 5 ms light pulses at 40 Hz in PRF every 1 minute in 4 laser intensities (1, 5, 10, 15 mW). We stimulated every condition (every optic fiber) 20 times (5-5-5-5 stimulation by intensities), and the experiment took about 30 min. During IL/Pf stimulation we used 30 Hz and 3 laser intensities (1, 5, 10 mW output laser intensity). After the experiments, we perfused the animals and identified the location of the virus injection and the optic fibers post hoc (see Histology).

Analysis

Statistics and reproducibility

In all behavioral, and electrophysiological experiments, mice were randomly grouped. In case of misplaced viral infections, the data points were excluded from the analysis. Animal numbers for each experiment are mentioned in the Figure legends. All data were checked for normality. Outliers were defined as Q1 - 3*IQR, Q3 + 3*IQR.

Statistical tests for juxtacellular analysis: Fig. 3f: Mood's median test, two sided; Fig. 4/d: Wilcoxon Signed-Rank Test, one sided; Supplementary Fig. 4: Wilcoxon Signed-Rank Test, one-sided; Fig. 6c: Wilcoxon Signed-Rank Test, two-sided; Supplementary Fig. 5: Mann-Whitney test, two-sided; Supplementary Fig. 7: Wilcoxon Signed-Rank Test, two-sided.

Statistical tests for *in vitro* analysis: Fig. 2e: Wilcoxon Signed-Rank Test; Fig. 2f: Wilcoxon Signed-Rank Test

Statistical test for behavior statistical analysis: Fig. 7c-d: Wilcoxon Signed-Rank Test, one-sided; Supplementary Fig. 8: Mann-Whitney test, two-sided Fig. 8c: Wilcoxon Signed-Rank Test, one-sided; Fig. 8f: Wilcoxon Signed-Rank Test, one-sided; Fig. 8, Supplementary 1c: Wilcoxon Signed-Rank Test, one-sided; Supplementary Fig. 9c: Wilcoxon Signed-Rank Test, one-sided; Supplementary Fig. 9d-e: Mann-Whitney test, two-sided.

Fiber density analysis

Following fluorescent immunostaining, we investigated the density of L5 fibers in the PRF. A map based on fiber density was created by FIJI software16[60]. A high-magnification

confocal micrograph was taken about PRF/GlyT2+ cells and M2/Cg L5 fibers (20x, NA: 0.75). The pictures were converted to 8-bit in depth then the brightest pixels of single optical slices of the original image stacks were projected into one plane to depict all of the labeled bright structures. These maximum intensity projections were smoothed by a Gauss filter with a radius of 40 pixels then the pixels were ordered according to their intensity values in 8 categories. The result is a pseudocolored, semi-quantitative map of the fiber density that enables the localization of the highest fiber density areas in a given image.

In vitro analysis

Sampling frequency was 40 kHz. Data was filtered at 3 kHz. All data were analyzed using routines developed in-house with Igor (Wavemetrics). Statistical comparisons were performed using either the Mann-Whitney test for unpaired values, or the Wilcoxon Signed-Rank test for paired sets of data, as indicated in the text. Statistical significance was set at 0.05. Results are given as mean ± s.e.m.

Analysis for juxtacellular recordings

All statistical analysis was performed in R Statistical Computing Software (R Core Team (2021). (R: A language and environment for statistical computing. R Foundation for Statistical Computing, Vienna, Austria. URL https://www.R-project.org/).

PFC photoactivation

To evaluate the effect of photoactivation the first APs following each stimulus were detected in a 40 ms window. They were distributed around ~10 ms peak with variable spread. Only APs in the [25th percentile - 1.5*IQR, 75th percentile + 1.5*IQR] & AP time

> 0 ms range were considered evoked response. APs occurring outside of this range were considered baseline firing activity and were excluded from further analysis.

Response probabilities were calculated as the number of evoked APs/number of stimuli*100 and plotted alongside the median latency values.

Spontaneous frontal cortical activity changes

To determine synchronous and desynchronous periods the raw LFP signal was filtered, down-sampled, and standardized. The power spectral density of each LFP signal was calculated, and the dominant frequency was determined. To find the synchronous and desynchronous periods of the cortical LFP signal, the standard deviation of the signal amplitude was calculated in overlapping sliding windows. The size of the sliding window was equal to the length of one cycle, and the overlap was half a cycle. The threshold for synchronous and desynchronous periods was placed halfway between the median and the 25th percentile.

The number of clusters was calculated in the synchronous and desynchronous periods and was statistically compared using the Wilcoxon test. Action potential clusters were determined by separating the two peaks at the minimum bimodal inter-spike interval histograms (ISI). The number of bins of the ISI was determined by the Freedman-Diaconis rule for optimal bin width; the window size was equal to the length of one cycle of the slow cortical oscillation. The mean cluster rate per LFP state was calculated by dividing the number of clusters by the length of the corresponding LFP states in every recording.

The mean firing rate (MFR) was calculated by dividing the sum number of action potentials divided by the sum lengths of the corresponding LFP states in every recording.

Thalamocortical neuronal activity

MFR before, during, and after stimuli were calculated as the sum number of APs divided by the sum length of each epoch. Based on the efficacy of the photo-stimulation the cells were divided into *weak* and *strong inhibition* categories. If the ratio of the number of APs +1s after and -1s before the stimulus was larger than 0.75 (number of spikes only dropped a little shortly after stimulus onset) the cell was categorized as *weak*ly inhibited, if it was smaller than 0.75 (big drop of spike numbers shortly after stimulus onset) the cell was categorized as *strong*ly inhibited.

Video analysis for behavior

To analyze the movements during the experiment we used Simple Mouse Tracker (SMT) downloaded from GitHub. SMT is a video tracker software based on Open CV that runs on any platform that supports Python. It is designed to track the body, head, and tail coordinates (X, Y) of a single-colour mouse over a homogeneous color background. https://github.com/joseaccruz/SimpleMouseTracker

After cleaning the tracking data (removing noise, outliers, and missing data) the before-stimulus speed and rotation of the animals were compared to the during-stimulus and -in the rotation experiments- to the after-stimulus periods.

To get the speed of the animals the Euclidean distance of the center (body) points across every 5th frame was calculated and converted to mm (scaling factor: 1.6 mm/pixel). To get the rotation of the animal the signed angle of the body-head vector was calculated across every frame and the mean rotation angles across frames were plotted.

For traveled distance plots every 5th frame (data point) was used (25 fps, scale: 1.6 pixel/mm). We calculated distances and average speed (mm/sec) across every 5th frame. Travelled distance (mm/sec) is averaged through the last second of the “before stimulus” category and the first second of the stimulus and the last 9 seconds of the stimulus. Travelled distance “after stimulus” is not included.

For rotation, we plotted every frame (data point). To show the animal’s movement trajectory during stimuli the head-center-tail body points were plotted, separately in non-stimulated and stimulated periods. We calculated vectors (based on head-body X-Y coordination) and measured the mean angle changes of every vector. After that, we divided that number by 360 to get which is the mean rotation angle between 2 frames (2 vectors) relative to one whole circle. The global angle threshold used in this file is 90. Grater rotation angles between consecutive frames are replaced by zero.

Data Availability

All relevant data supporting the findings of this study are available within the article and its supplementary materials. Additionally, source data and codes will be deposits in an appropriate public structured data repositories to ensure accessibility and future use.

Full access to the data will be granted upon publication to enable comprehensive assessment and validation of our results. In compliance with our commitment to open science, we are prepared to provide full access to the data, should it be required for the peer review.

References

1. Leiras, R., Cregg, J. M. & Kiehn, O. Brainstem Circuits for Locomotion. *Annu Rev Neurosci* **45**, 63–85 (2022).

2. Arber, S. & Costa, R. M. Networking brainstem and basal ganglia circuits for movement. *Nature Reviews Neuroscience 2022 23:6* **23**, 342–360 (2022).

3. Smith, Y., Raju, D. V., Pare, J. F. & Sidibe, M. The thalamostriatal system: A highly specific network of the basal ganglia circuitry. *Trends in Neurosciences* vol. 27 520–527 Preprint at https://doi.org/10.1016/j.tins.2004.07.004 (2004).

4. Cui, G. *et al.* Concurrent activation of striatal direct and indirect pathways during action initiation. *Nature* **494**, 238–242 (2013).

5. Díaz-Hernández, E. *et al.* The Thalamostriatal Projections Contribute to the Initiation and Execution of a Sequence of Movements. (2018) doi:10.1016/j.neuron.2018.09.052.

6. Hintiryan, H. *et al.* The mouse cortico-striatal projectome. *Nature Neuroscience 2016 19:8* **19**, 1100–1114 (2016).

7. Hunnicutt, B. J. *et al.* A comprehensive excitatory input map of the striatum reveals novel functional organization. *Elife* **5**, (2016).

8. Alexander, G. E., DeLong, M. R. & Strick, P. L. Parallel Organization of Functionally Segregated Circuits Linking Basal Ganglia and Cortex.

https://doi.org/10.1146/annurev.ne.09.030186.002041 **VOL. 9**, 357–381 (2003).

9. Gerfen, C. R. Synaptic organization of the striatum. *J Electron Microsc Tech* **10**, 265–281 (1988).

10. Kemp, J. M. & Powell, T. P. The structure of the caudate nucleus of the cat: light and electron microscopy. *Philosophical Transactions of the Royal Society of London. B, Biological Sciences* **262**, 383–401 (1971).

11. Kultas-ilinsky, K., Ilinsky, I., Warton, S. & Smith, K. R. Fine structure of nigral and pallidal afferents in the thalamus: An em autoradiography study in the cat. *Journal of Comparative Neurology* **216**, 390–405 (1983).

12. Ilinsky, I. A., Yi, H. & Kultas-Ilinsky, K. Mode of Termination of Pallidal Afferents to the Thalamus: A Light and Electron Microscopic Study With Anterograde Tracers and Immunocytochemistry in Macaca mulatta. *J. Comp. Neurol* **386**, 601–612 (1997).

13. Bodor, Á. L., Giber, K., Rovó, Z., Ulbert, I. & Acsády, L. Structural correlates of efficient GABAergic transmission in the basal ganglia-thalamus pathway. *Journal of Neuroscience* **28**, (2008).

14. Ueki, A. The mode of nigro-thalamic transmission investigated with intracellular recording in the cat. *exp brain res* **49**, 116–124 (1983).

15. Chevalier, G. & Deniau, J. M. Inhibitory nigral influence on cerebellar evoked responses in the rat ventromedial thalamic nucleus. *Exp Brain Res* **48**, 369–376 (1982).

16. Goldberg, J. H., Farries, M. A. & Fee, M. S. Basal ganglia output to the thalamus: still a paradox. *Trends Neurosci* **36**, 695–705 (2013).

17. Pare, D. & Smith, Y. Thalamic Collaterals of Corticostriatal Axons: Their Termination Field and Synaptic Targets in Cats. *J Comp Neurol* 372–551 (1996) doi:10.1002/(SICI)1096-9861(19960902)372:4.

18. Konnova, E. A. & Swanberg, M. Animal Models of Parkinson's Disease. *Parkinson's Disease: Pathogenesis and Clinical Aspects* 83–106 (2018) doi:10.15586/CODONPUBLICATIONS.PARKINSONSDISEASE.2018.CH5.

19. Tecuapetla, F., Matias, S., Dugue, G. P., Mainen, Z. F. & Costa, R. M. Balanced activity in basal ganglia projection pathways is critical for contraversive movements. *Nat Commun* **5**, 1–10 (2014).

20. Thanos, P. K., Jhamandas, K. & Beninger, R. J. N-Methyl-d-asparate unilaterally injected into the dorsal striatum of rats produces contralateral circling: antagonism by 2-amino-7-phosphonoheptanoic acid and cis-flupenthixol. *Brain Res* **589**, 55–61 (1992).

21. Brasted, P. J., Humby, T., Dunnett, S. B. & Robbins, T. W. Unilateral lesions of the dorsal striatum in rats disrupt responding in egocentric space. *Journal of Neuroscience* **17**, 8919–8926 (1997).

22. Boix, J., Padel, T. & Paul, G. A partial lesion model of Parkinson's disease in mice – Characterization of a 6-OHDA-induced medial forebrain bundle lesion. *Behavioural Brain Research* **284**, 196–206 (2015).

23. Schwarting, R. K. W. & Huston, J. P. The unilateral 6-hydroxydopamine lesion model in behavioral brain research. Analysis of functional deficits, recovery and treatments. *Prog Neurobiol* **50**, 275–331 (1996).

24. Masini, D. & Kiehn, O. Targeted activation of midbrain neurons restores locomotor function in mouse models of parkinsonism. *Nat Commun* **13**, (2022).

25. Cregg, J. M. *et al.* Brainstem neurons that command mammalian locomotor asymmetries. *Nat Neurosci* **23**, 730–740 (2020).

26. Josset, N. *et al.* Distinct Contributions of Mesencephalic Locomotor Region Nuclei to Locomotor Control in the Freely Behaving Mouse. *Current Biology* **28**, 884-901.e3 (2018).

27. Caggiano, V. *et al.* Midbrain circuits that set locomotor speed and gait selection. *Nature 2018 553:7689* **553**, 455–460 (2018).

28. Roseberry, T. K. *et al.* Cell-Type-Specific Control of Brainstem Locomotor Circuits by Basal Ganglia. *Cell* **164**, 526–537 (2016).

29. Giber, K. *et al.* A subcortical inhibitory signal for behavioral arrest in the thalamus. *Nat Neurosci* **18**, 562–568 (2015).

30. Zeilhofer, H. U. *et al.* Glycinergic neurons expressing enhanced green fluorescent protein in bacterial artificial chromosome transgenic mice. *J Comp Neurol* **482**, 123–141 (2005).

31. Halassa, M. M. & Acsády, L. Thalamic Inhibition: Diverse Sources, Diverse Scales. *Trends Neurosci* **39**, 680–693 (2016).

32. McElvain, L. E. *et al.* Specific populations of basal ganglia output neurons target distinct brain stem areas while collateralizing throughout the diencephalon. *Neuron* **109**, 1721-1738.e4 (2021).

33. Pinault, D. A novel single-cell staining procedure performed in vivo under electrophysiological control: Morpho-functional features of juxtacellularly labeled thalamic cells and other central neurons with biocytin or Neurobiotin. *J Neurosci Methods* **65**, 113–136 (1996).

34. Barthó, P. *et al.* Cortical Control of Zona Incerta. *The Journal of Neuroscience* **27**, 1670 (2007).

35. Groh, A. *et al.* Convergence of cortical and sensory driver inputs on single thalamocortical cells. *Cereb Cortex* **24**, 3167–3179 (2014).

36. Economo, M. N. *et al.* A platform for brain-wide imaging and reconstruction of individual neurons. *Elife* **5**, (2016).

37. Arnts, H. *et al.* The intralaminar thalamus: a review of its role as a target in functional neurosurgery. *Brain Commun* (2023) doi:10.1093/BRAINCOMMS/FCAD003.

38. Tecuapetla, F., Jin, X., Lima, S. Q. & Costa, R. M. Complementary Contributions of Striatal Projection Pathways to Action Initiation and Execution. *Cell* **166**, 703–715 (2016).

39. Foster, N. N. *et al.* The mouse cortico–basal ganglia–thalamic network. *Nature* **598**, 188 (2021).

40. Fujii, N. & Graybiel, A. M. Time-varying covariance of neural activities recorded in striatum and frontal cortex as monkeys perform sequential-saccade tasks. *Proc Natl Acad Sci U S A* **102**, 9032–9037 (2005).

41. Pidoux, M., Mahon, S., Deniau, J. M. & Charpier, S. Integration and propagation of somatosensory responses in the corticostriatal pathway: an intracellular study in vivo. *J Physiol* **589**, 263–281 (2011).

42. Peters, A. J., Fabre, J. M. J., Steinmetz, N. A., Harris, K. D. & Carandini, M. Striatal activity topographically reflects cortical activity. *Nature 2021 591:7850* **591**, 420–425 (2021).

43. Paz, J. T., Chavez, M., Saillet, S., Deniau, J.-M. & Charpier, S. Activity of ventral medial thalamic neurons during absence seizures and modulation of cortical paroxysms by the nigrothalamic pathway. *J Neurosci* **27**, 929–41 (2007).

44. Catanese, J. & Jaeger, D. Premotor Ramping of Thalamic Neuronal Activity Is Modulated by Nigral Inputs and Contributes to Control the Timing of Action Release. *J Neurosci* **41**, 1878–1891 (2021).

45. Wang, Y. *et al.* A cortico-basal ganglia-thalamo-cortical channel underlying short-term memory. *Neuron* **0**, 1–14 (2021).

46. Telgkamp, P., Padgett, D. E., Ledoux, V. A., Woolley, C. S. & Raman, I. M. Maintenance of high-frequency transmission at purkinje to cerebellar nuclear synapses by spillover from boutons with multiple release sites. *Neuron* **41**, 113–126 (2004).

47. Halassa, M. M. & Acsády, L. Thalamic Inhibition: Diverse Sources, Diverse Scales. *Trends Neurosci* **39**, 680–693 (2016).

48. McElvain, L. E. *et al.* Specific populations of basal ganglia output neurons target distinct brain stem areas while collateralizing throughout the diencephalon. *Neuron* **109**, 1721-1738.e4 (2021).

49. Sedelis, M., Schwarting, R. K. W. & Huston, J. P. Behavioral phenotyping of the MPTP mouse model of Parkinson's disease. *Behavioural Brain Research* **125**, 109–125 (2001).

50. Morrissette, A. E. *et al.* Unilateral Optogenetic Inhibition and Excitation of Basal Ganglia Output Affect Directional Lick Choices and Movement Initiation in Mice. *Neuroscience* **423**, 55–65 (2019).

51. Mandelbaum, G. *et al.* Distinct Cortical-Thalamic-Striatal Circuits through the Parafascicular Nucleus. *Neuron* **102**, 636-652.e7 (2019).

52. Berendse, H. W. & Groenewegen, H. J. Organization of the thalamostriatal projections in the rat, with special emphasis on the ventral striatum. *J Comp Neurol* **299**, 187–228 (1990).

53. Bouvier, J. *et al.* Descending Command Neurons in the Brainstem that Halt Locomotion. *Cell* **163**, 1191 (2015).

54. Cregg, J. M. *et al.* Brainstem neurons that command mammalian locomotor asymmetries. *Nat Neurosci* **23**, 730–740 (2020).

55. Gallager, D. W. & Pert, A. Afferents to brain stem nuclei (brain stem raphe, nucleus reticularis pontis caudalis and nucleus gigantocellularis) in the rat as demonstrated by microiontophoretically applied horseradish peroxidase. *Brain Res* **144**, 257–275 (1978).

56. Hermann, D. M., Luppi, P. H., Peyron, C., Hinckel, P. & Jouvet, M. Afferent projections to the rat nuclei raphe magnus, raphe pallidus and reticularis gigantocellularis pars α demonstrated by iontophoretic application of choleratoxin (subunit b). *J Chem Neuroanat* **13**, 1–21 (1997).

57. Hajnik, T., Lai, Y. Y. & Siegel, J. M. Atonia-Related Regions in the Rodent Pons and Medulla. *J Neurophysiol* **84**, 1942 (2000).

58. Bar-Gad, I., Morris, G. & Bergman, H. Information processing, dimensionality reduction and reinforcement learning in the basal ganglia. *Prog Neurobiol* **71**, 439–473 (2003).

59. Kiehn, O. Decoding the organization of spinal circuits that control locomotion. *Nat Rev Neurosci* **17**, 224 (2016).

60. Schindelin, J. *et al.* Fiji: an open-source platform for biological-image analysis. *Nature Methods 2012 9:7* **9**, 676–682 (2012).